Interstellar Polycyclic Aromatic Hydrocarbon Molecules*

A.G.G.M. Tielens

Space Sciences Division, NASA Ames Research Center, Moffett Field, California 94035; email: tielens@astro.rug.nl

Annu. Rev. Astron. Astrophys. 2008. 46:289–337

The *Annual Review of Astronomy and Astrophysics* is online at astro.annualreviews.org

This article's doi:
10.1146/annurev.astro.46.060407.145211

0066-4146/08/0922-0289$20.00

Key Words

infrared emission features, infrared spectroscopy, interstellar chemistry, interstellar medium, interstellar molecules

Abstract

Large polycyclic aromatic hydrocarbon (PAH) molecules carry the infrared (IR) emission features that dominate the spectra of most galactic and extragalactic sources. This review surveys the observed mid-IR characteristics of these emission features and summarizes laboratory and theoretical studies of the spectral characteristics of PAHs and the derived intrinsic properties of emitting interstellar PAHs. Dedicated experimental studies have provided critical input for detailed astronomical models that probe the origin and evolution of interstellar PAHs and their role in the universe. The physics and chemistry of PAHs are discussed, emphasizing the contribution of these species to the photoelectric heating and the ionization balance of the interstellar gas and to the formation of small hydrocarbon radicals and carbon chains. Together, these studies demonstrate that PAHs are abundant, ubiquitous, and a dominant force in the interstellar medium of galaxies.

1. INTRODUCTION

In the mid-1970s, ground-based and airborne studies revealed relatively broad emission features in mid-infrared (mid-IR) spectra of bright HII regions, planetary nebulae (PNe), and reflection nebulae. The opening up of the IR sky by the Infrared Space Observatory (ISO) and the Spitzer Space Observatory has revealed the incredible richness of the mid-IR spectrum (**Figure 1**). Additionally, the high sensitivity of these space-based observations has demonstrated that these IR emission features are ubiquitous and are present in almost all objects, including HII regions, reflection nebulae, young stellar objects, PNe, postasymptotic giant branch (AGB) objects, nuclei

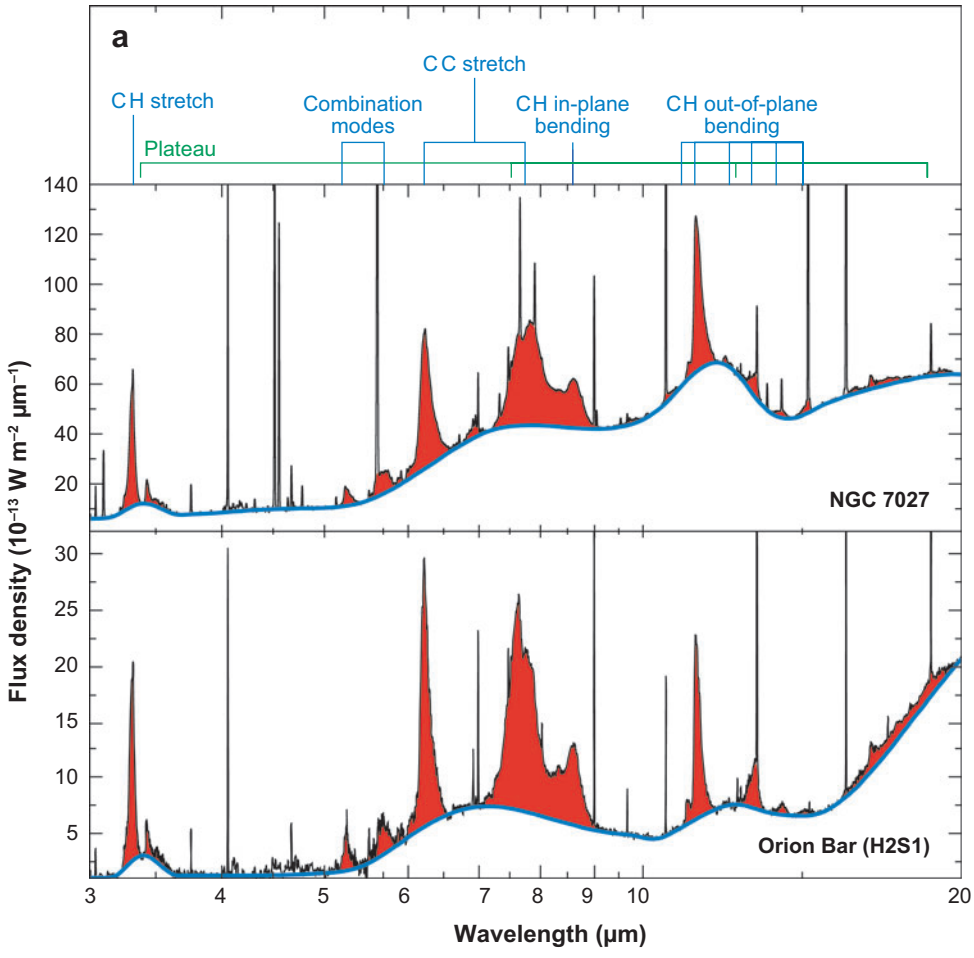

Figure 1

(*a*) The mid-infrared spectra of the photodissociation region in the Orion Bar and in the planetary nebulae NGC 7027 are dominated by a rich set of emission features. These features are labeled with the vibrational modes of polycyclic aromatic hydrocarbon molecules at the top. Figure adapted from Peeters et al. 2002. (*b*) Three spectra selected from the SINGS sample of nuclei of nearby galaxies. The measured νI_ν in units of 10^{-6} W m^{-2} sr^{-1} is shown as a function of rest wavelength in micrometers. Figure taken from Smith et al. 2007. Note the relative intensity variations between the CC and CH modes and among the CH out-of-plane bending modes. The narrow features are atomic or ionic lines originating in the HII region or photodissociation region.

of galaxies, and ultraluminous infrared galaxies (ULIRGs) (Verstraete et al. 1996, Genzel et al. 1998, Moutou et al. 1999, Hony et al. 2001, Verstraete et al. 2001, Peeters et al. 2002, Acke & van den Ancker 2004, Brandl et al. 2006, Geers et al. 2006, Armus et al. 2007). Moreover, the IR cirrus, the surfaces of dark clouds, and the general interstellar medium (ISM) of galaxies are set aglow in these IR emission features (Mattila et al. 1996, Burton et al. 2000, Abergel et al. 2002, Regan et al. 2004, Smith et al. 2007). These features are (almost) universally attributed to the IR fluorescence of far-ultraviolet (FUV)-pumped polycyclic aromatic hydrocarbon (PAH) molecules, containing ~50 C atoms (Sellgren 1984; Allamandola, Tielens & Barker 1989; Puget

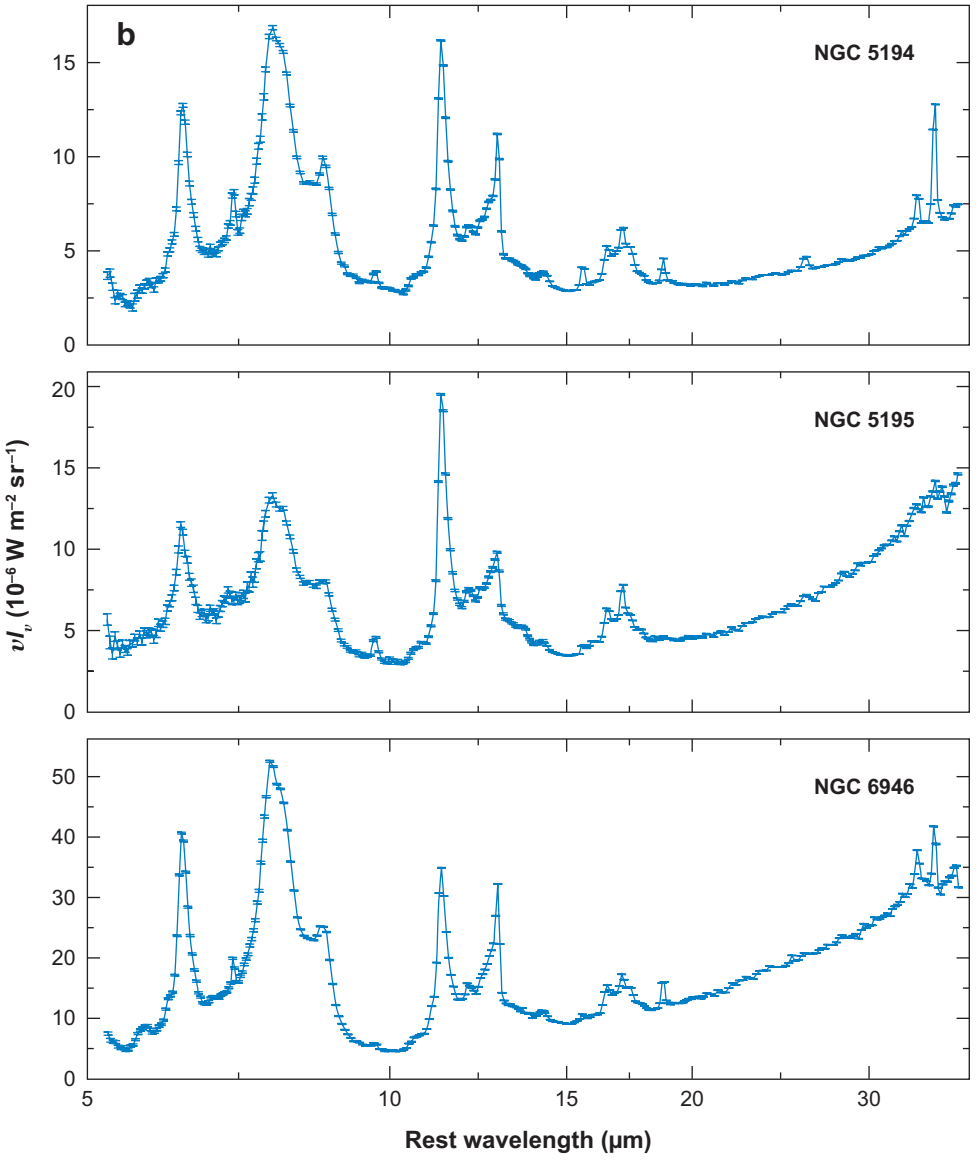

Figure 1

(*Continued*)

& Leger 1989). This assignment is based on an energetics argument: Small species have a low heat capacity and get so hot upon absorption of a single photon that they emit in the mid-IR, even far from the illuminating star. In addition, the high feature-to-continuum ratio implicates a molecular rather than solid-state origin. Finally, the profile of many of these bands is characteristic of anharmonicity associated with molecular emission. PAHs are abundant—10^{-7} by number relative to hydrogen—and ubiquitous in the ISM. Obviously, PAHs are an important component of the ISM, and their presence has major ramifications. In particular, these species dominate the heating of neutral gas and the ionization balance in molecular clouds; hence they influence the phase structure of the ISM, the ion-molecule chemistry that builds up simple gas-phase species, and the ambipolar diffusion process that sets the stage for star formation. The IR features are very bright in regions powered by young massive stars, such as HII regions. Hence, the IR emission features are generally taken to be tracers of galactic (massive) star formation in the local, as well as more distant, universe (Genzel et al. 1998, Lutz et al. 2007, Rigby et al. 2007, Pope et al. 2007).

Interstellar PAHs have been reviewed by Puget & Leger (1989) and Allamandola, Tielens & Barker (1989). There has been much progress over the past 20 years. First, ISO and Spitzer have allowed systematic studies of the mid-IR window. The smaller Midcourse Space Experiment and Infrared Telescope in Space missions as well as the birth of the 8-m class, ground-based telescope era have provided additional observational impetus. This has created a wealth of observational detail in the spatial and spectral behavior of the IR emission features in space. Second, dedicated laboratory and theoretical efforts have provided deep insight into the intrinsic spectral and chemical characteristics of interstellar PAH molecules. Third, based on this experimental and theoretical understanding, models for the emission of astronomical sources have reached a level of maturation that starts to allow detailed comparison with observations. Similarly, models for the chemistry involved have provided much insight into the formation and evolution of interstellar PAHs. With much data still unexplored in the Spitzer archives, and the Stratospheric Observatory for Infrared Astronomy (SOFIA) and the James Webb Space Telescope missions around the corner, the future looks bright from an observational point of view. Likewise, more and more experimental and theoretical groups are focusing on elucidating the properties of interstellar PAHs. Below, I intend to convey the exciting progress that has been made, as well as point out some key questions.

2. OBSERVED CHARACTERISTICS OF INFRARED EMISSION FEATURES

2.1. The Infrared Emission Features

The interstellar IR emission spectrum is incredibly rich and shows a wealth of detail. It is dominated by major emission features at 3.3, 6.2, 7.7, 8.6, 11.2, 12.7, and 16.4 μm (**Figure 1**). In addition, there are weaker features at 3.4, 3.5, 5.25, 5.75, 6.0, 6.9, 7.5, 10.5, 11.0, 13.5, 14.2, 17.4, and 18.9 μm. These features are perched on broad emission plateaus from 3.2 to 3.6, 6 to 9, 11 to 14, and 15 to 19 μm. Moreover, many of the well-known features shift in peak position, vary in width, and/or show substructure, revealing a sensitivity to the local physical conditions (see Sections 2.2.1 and 2.2.2).

The IR emission features dominate the mid-IR spectra of almost all objects with associated dust and gas and illuminated by UV photons. **Figure 2** shows a composite image of the Orion star-forming regions obtained by the Spitzer infrared array camera. The well-known HII region of the Orion nebula (M42) and its companion HII region M43 are located near the center of the image. The prominent ionization front, the Orion Bar, is also evident to the southwest of M42. In this region, the IR emission features trace the front of the photodissociation regions (PDRs),

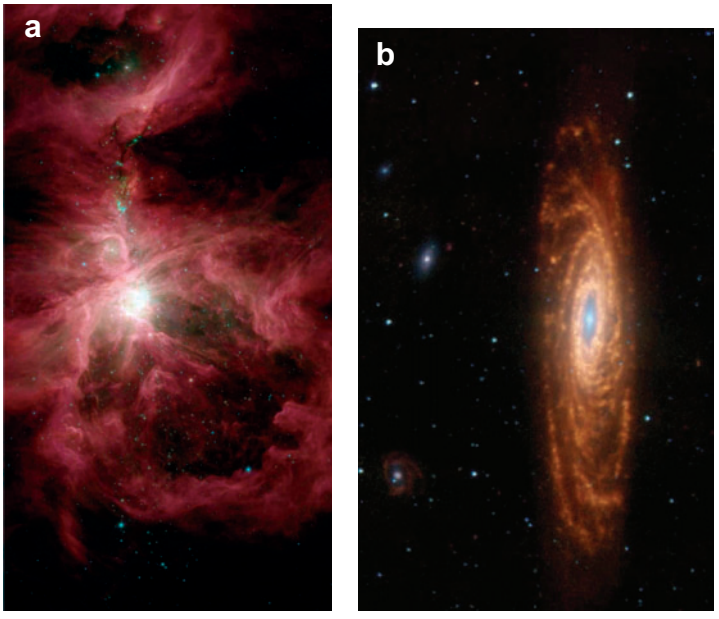

Figure 2

Composite mid-infrared images of the Orion star-forming region (*a*) and NGC 7331, the twin of the Milky Way (*b*), obtained with the infrared array camera on the Spitzer Space Telescope. The 8-μm image (*red*) traces primarily the 7.7-μm feature. The 4.5-μm image (*green*) shows ionized gas and dust. Stars appear at 3.6 μm (*blue*). Images courtesy of NASA/JPL-Caltech.

which separates the ionized gas from the surrounding molecular gas (e.g., Tielens et al. 1993). Although the carriers of the IR emission features apparently do not survive in the ionized gas (as **Figure 2** clearly illustrates), the whole cloud is set aglow in the emission of the 7.7-μm band pumped by the newly formed stellar association, creating the beautiful swirls of material.

The IR emission features were initially discovered in objects with high surface brightness. However, the Infrared Astronomical Satellite mission demonstrated the widespread presence of emission at mid-IR wavelengths associated with (IR) cirrus in the diffuse ISM (Low et al. 1984). Although ISOPHOT observations of the galactic cirrus and of the edge-on twin of the Milky Way, NGC 891, revealed that the spectrum of this diffuse mid-IR emission is dominated by the IR emission features (Mattila et al. 1996), it took the extraordinary sensitivity of the Spitzer infrared array camera to make us fully appreciate the widespread dominance of the mid-IR emission (Regan et al. 2004). As an example, **Figure 2** shows a composite image of the well-known galaxy NGC 7331 (often considered a twin of the Milky Way) at mid-IR wavelengths. However, the spiral structure is well traced by the 7.7-μm emission, which is particularly bright in regions in which massive stars illuminate their surroundings. All spiral galaxies show similar widespread mid-IR emission [see Soifer, Helou & Werner (2008) for a similarly beautiful mid-IR image of the whirlpool galaxy M51]. The IR emission features clearly are an important and widespread component of the ISM of galaxies.

2.2. Spectral Variations

Observed spectral variations can be separated into two categories: (*a*) variations in the relative strength of the different IR emission features and (*b*) variations in the peak positions and profiles of the features.

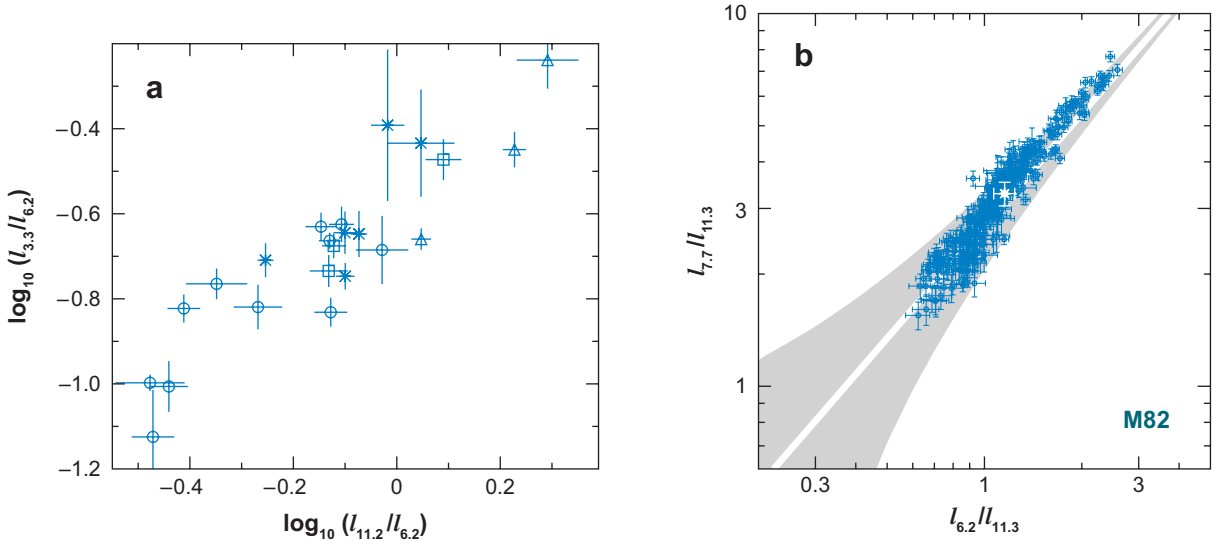

Figure 3

(*a*) A comparison of the strength of the 3.3-μm CH stretching band with that of the 11.3-μm CH out-of-plane bending band, both normalized to the 6.2-μm CC stretching band. The CH modes correlate much better with each other than with the CC modes. Similarly, the 6.2-μm and 7.7-μm CC modes correlate much better with each other than with the CH modes. Figure taken from Hony et al. 2001. (*b*) Variations in the relative strength of the CH modes to the CC modes in the starburst galaxy M82. The gray area denotes the correlation obtained for the bands in the integrated spectra of a large sample of galactic and extragalactic sources. Figure taken from Galliano et al. 2008.

2.2.1. Relative intensities. Observations of variations in relative strength stem back to the Kuiper Airborne Observatory and ground-based studies. Specifically, the relative strength of the 3.4-μm to the 3.3-μm band, the 11.3-μm to the 8.6-μm band, and the 7.7-μm emission feature to its underlying plateau varies systematically across the Orion Bar PDR (Bregman et al. 1989, Geballe et al. 1989, Joblin et al. 1996). ISO and Spitzer have provided us with large coherent data sets that firmly establish the widespread nature of these variations. **Figure 3** summarizes intensity variations between the CC and CH modes in a sample of galactic objects (Hony et al. 2001), whereas **Figure 1** illustrates similar variations in spectra of galaxies (Smith et al. 2007). Such variations have also been observed within individual objects, including the reflection nebula NGC 1333 SVS 3; the HII regions S106, the Orion Bar, and M17; and a variety of galaxies (**Figure 3**) (Joblin et al. 2000, Verstraete et al. 2001, Bregman & Temi 2005, Galliano et al. 2008).

2.2.2. Profile variations. The profiles of the IR emission features show pronounced variations from source to source (**Figure 4**). Although the peak position and profiles of the CH modes show only minor variations, those of the CC modes in the 5–9-μm region are highly variable, even in relatively low-resolution data. Peeters et al. (2002) have classified these profiles into three categories: A, B, and C. Profile A peaks at 6.2 μm and shows a sharp blue rise and a red tail, whereas profile B and C peak at longer wavelengths and are more symmetric. We can also classify the 7.7-μm band into three categories. The A and B categories differ largely in the relative strength of subcomponents at 7.6 and 7.8 μm. For the C category, this band seems to have shifted all the way to 8.2 μm. For the A and B categories, the variations seem to span the range continuously. There are few C-type sources; hence it is difficult to ascertain whether they form a completely independent category or are continuously connected to the A- and B-type sources. The variations

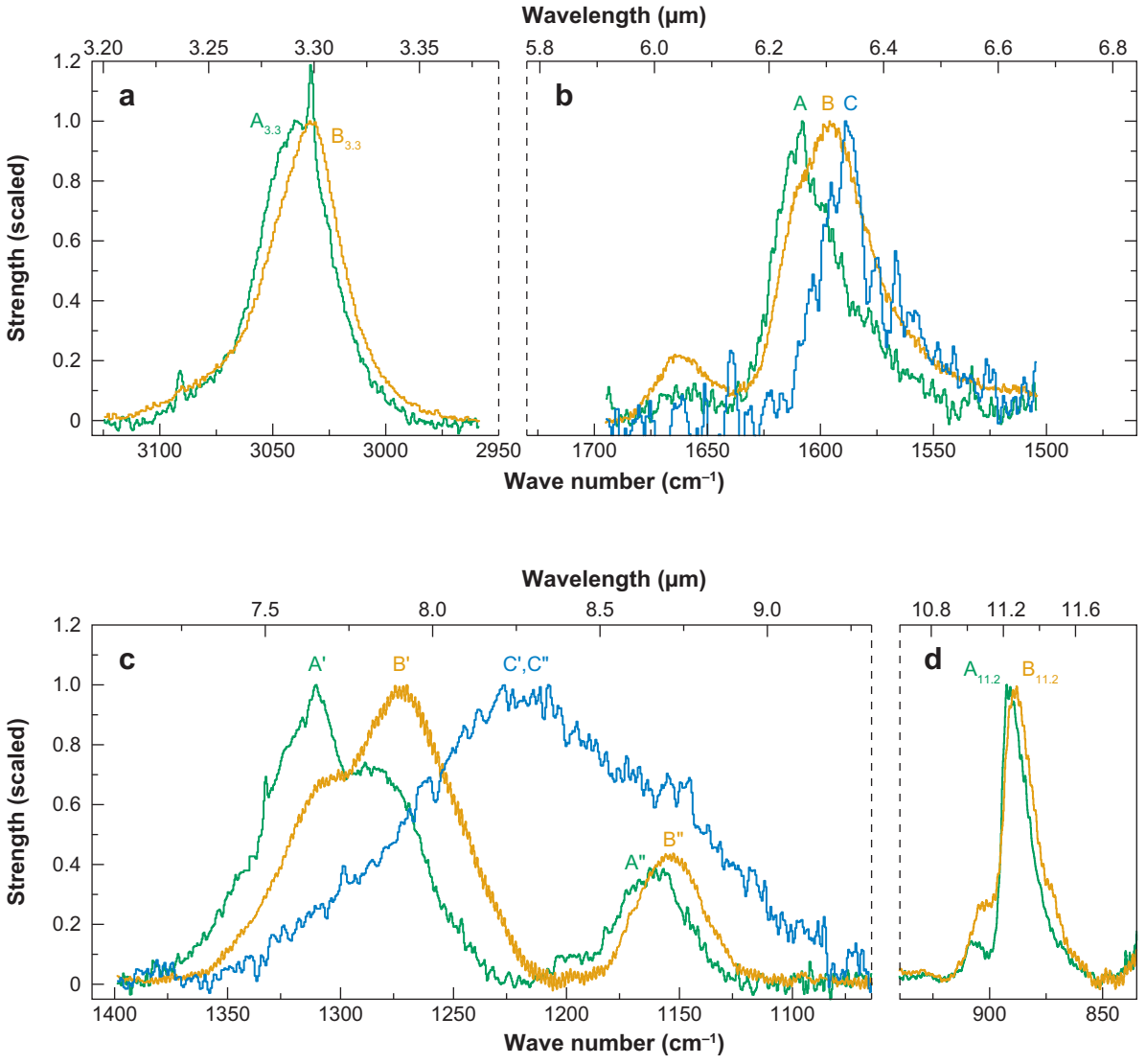

Figure 4

An overview of the source-to-source variations in the position and profile of IR emission features. The CH modes in the 3-μm and the 10–15-μm region show only minor variations. In contrast, large variations are evident for the CC modes in the 6–9-μm range. For all features, class A peaks at the shortest wavelengths (*green line*), and class B (*orange*) peaks at longer wavelengths. The CC modes of class C (*blue*) peak at even longer wavelengths. Figure taken from van Diedenhoven et al. 2004.

in the profiles of the CC modes are correlated: The 6.2-μm and 7.7-μm bands shift in the same way between sources. In contrast, the variations in the peak positions of the CH and CC mode are not necessarily correlated (van Diedenhoven et al. 2004).

Finally, these variations are linked to the type of source. Class A sources consist of interstellar material illuminated by a star, including HII regions, reflection nebulae, and the general ISM of the Milky Way and other galaxies. Class B sources are associated with circumstellar material and include PNe and a variety of post-AGB objects, as well as Herbig AeBe stars. Class C sources

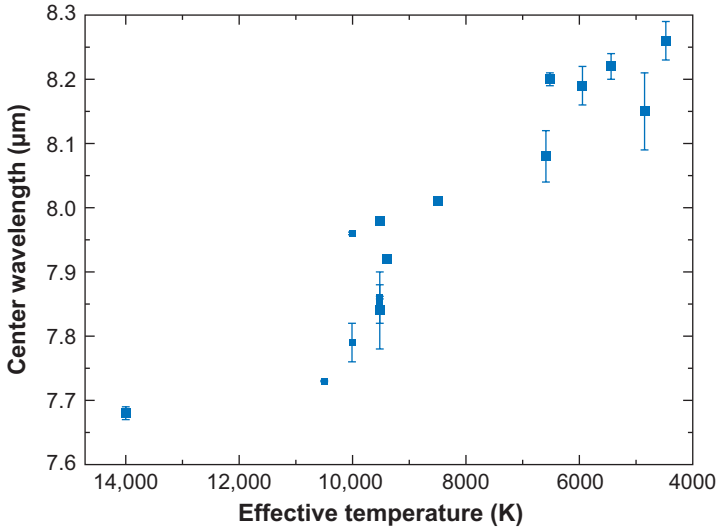

Figure 5

The mean position of the 7.7-μm band as a function of the effective temperature of the exciting star (Sloan et al. 2007; C. Boersma et al., manuscript in preparation). Mean positions correspond to the wavelength in which equal amounts of integrated flux are to shorter and longer wavelengths. All interstellar medium sources have similar peak positions. Because the far-infrared radiation field is largely independent of T_{eff} for these hot sources, a single point is shown. In the Peeters classification, this point is class A. The transition to class B falls at approximately 10,000 K, whereas class C occurs at the lowest temperatures, ~6000 K.

are limited to a few extreme carbon-rich post-AGB objects. Sloan et al. (2007) pointed out an intriguing relationship between the peak position of the 7.7-μm band and to a lesser extent the 11.2-μm band and the effective temperature of the exciting star (**Figure 5**) (see also C. Boersma et al., manuscript in preparation). Although this figure might be interpreted as a global trend in the peak position, there seems to be rapid transition in the peak position at approximately 10,000 K from class A to class B—separating the ISM sources from the Herbig stars—and then again at approximately 6000 K from class B to class C—separating the Herbig stars from the post-AGB objects. Only two young stellar objects fall near the class C position: HD 135344 and SU Aur. The Herbig star HD 135344 ($\lambda \simeq 8.08$ μm, $T_{eff} \simeq 6600$ K) seems to link classes B and C, but that point refers to relatively low-resolution Infrared Spectrograph (IRS) spectral data. The peak position of the T Tauri star SU Aur ($\lambda \simeq 8.19$ μm, $T_{eff} \simeq 5900$ K) falls among the post-AGB objects but is uncertain because this band is weak and perched on a strong silicate feature. The rapid transition between the ISM sources and the Herbig stars is typified by three Herbig stars: TY CrA, HD 97048, and HD 100546. All three are B9 stars, yet TY CrA has a typical ISM position, and, indeed, most of the emission originates from the surrounding reflection nebula, whereas HD 100546 has a class B profile and its emission comes solely from the circumstellar disk. The profile of HD 97048 is an approximately 50:50 mix of profiles A and B and originates from both the disk and the surrounding cloud (Habart et al. 2006, Doucet et al. 2007). Thus, in addition to or rather than the effective temperature, the shift from class A may be connected to the presence of circumstellar material (Van Kerckhoven 2002; C. Boersma et al., manuscript in preparation).

2.2.3. Principal component analysis. Rapacioli, Joblin & Boissel (2005) have taken a somewhat different approach, using principal component analysis on spatial-spectral ISOCAM maps of two reflection nebula. This analysis identified three different components (**Figure 6**). The first is

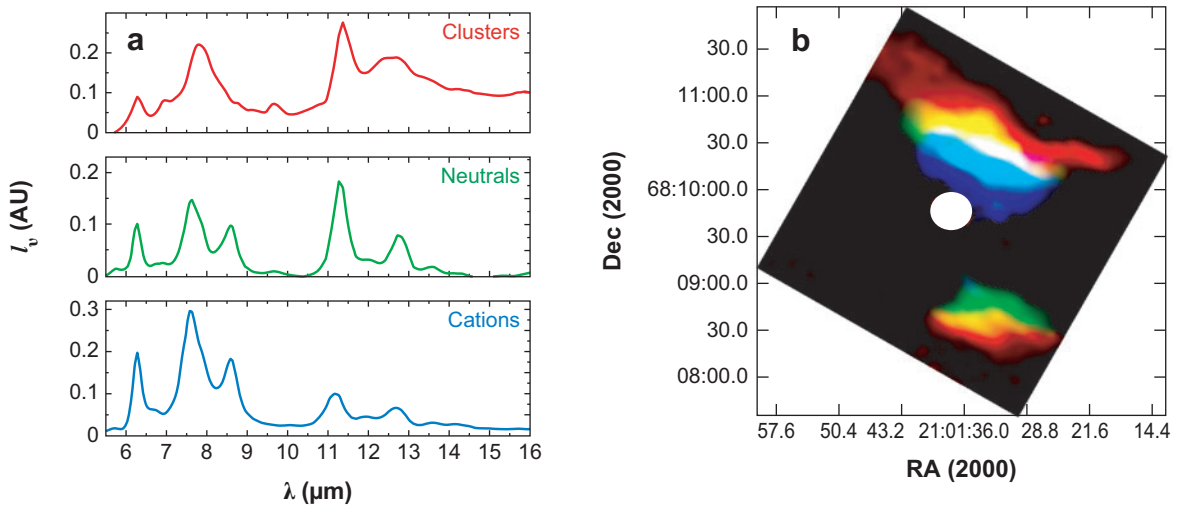

Figure 6

(*a*) Three identified components in the singular value decomposition analysis of ISOCAM spectral-spatial maps of NGC 7023. The components are normalized by their integrated intensity. (*b*) These components show different spatial distributions in this source and have been attributed to ionic (*blue*) and neutral (*green*) polycyclic aromatic hydrocarbon molecules and clusters (*red*), respectively. In the color scheme used, red and green combine to yellow. Figure taken from Rapacioli, Joblin & Boissel 2005 and Berné et al. 2008.

characterized by strong CC modes relative to the CH modes, whereas this ratio is reversed for the second component. Neither component shows discernable continuum emission. The third component consists of a continuum with weaker and broader IR emission features. Moreover, the 7.7-μm feature peaks at longer wavelengths (e.g., 7.8 rather than 7.6 μm). These components can be separated in this data because they have different spatial distributions within these nebulae [e.g., with distance from the illuminating star (**Figure 6**)]. These results agree with the analysis of the reflection nebulae Ced 201 (Cesarsky et al. 2000). Three distinct emission components were also extracted from Spitzer IRS spectral-image data cubes of three reflection nebulae using a blind-signal separation method (Berné et al. 2007). The characteristics of these components are similar to those derived from the ISOCAM study: one component with a strong continuum and weak, broad emission features and two components with emission features and no continuum, differing in the relative strength of the CH and CC modes. These three components have been attributed to PAH cations, PAH neutrals, and PAH clusters, respectively. The neutral component does show more spectral activity in the 6–9-μm region than we might expect based on laboratory studies of (small) PAHs (see Section 4.2.1). The analyzed region possibly does not contain a zone of pure neutral PAH emission. Alternatively, this reflects the effect of size on the intrinsic spectrum of neutral PAHs (see Section 4.2.1).

2.3. Spectral Analysis

In the analysis of the observed strength of the IR emission features, various approximations are often made. These approximations are based on underlying assumptions regarding the characteristics of the various components contributing to the IR spectrum that are normally not explicitly articulated. Generally, all analyses assume the presence of a featureless continuum spanning the full observed wavelength range. This continuum is thought to arise in very small grains, and the characteristic temperature and absolute flux level are determined by the fit to the observations.

Although the detailed assumptions among the different groups differ, the results are very similar.

Approaches to the analysis of the properties of the IR emission features differ in a more substantial way. Specifically, Gaussian as well as Lorentzian (and sometimes confusingly Drude) profiles have been assumed. A truly isolated harmonic oscillator has a Lorentzian emission profile. However, an excited species can be perturbed by collisions during the emission process, which may have major effects on the emission profile. The IR emission features originate in highly vibrationally excited species on a timescale (microseconds) that is long compared to the vibration period of the modes (picoseconds) and the timescale for intramolecular energy transfer (nanoseconds). Hence, the emitting vibrating atoms find themselves in a constantly changing interaction potential—caused by this population of background excitations—which leads to anharmonic shifts of the peak position and characteristic red-shaded profiles (Barker, Allamandola & Tielens 1987; Cook & Saykally 1998; Pech, Joblin & Boissel 2002). In contrast, the Gaussian approach attributes the width of IR emission features to the blending of a set of intrinsically relatively narrow Lorentzian profiles (e.g., Voigt profiles for which the damping contribution can be ignored compared with the contribution of the Gaussian core). The set of individual oscillators contributing to an emission feature reflects then the presence of a large and diverse family of interstellar PAH molecules whose detailed peak position is assumed to be randomly distributed around a mean position.

Peeters et al. (2002) has decomposed the spectral features in relatively narrow IR emission bands perched on broad underlying plateaus. The profile of the former was represented by Gaussians whose parameters (peak position and width) were fitted to the data, whereas for the latter a spline was fitted to specific wavelengths. In contrast, Smith et al. (2007) have adopted a set of Lorentzian profiles. The strength of the derived emission features is sensitive to these assumptions. In particular, for a given width, Lorentzian profiles have intrinsically much stronger (damping) wings than Gaussian profiles, and as a result, the Lorentzian approach leaves no room for broad underlying plateaus in their spectral fits. Neither approach is well grounded in reality. The intrinsic profiles of highly vibrationally excited PAHs are anharmonic and red-shaded in nature. In addition, there is observational evidence for broad underlying plateaus that behave independently from the IR emission features, and these are difficult to accommodate in the Lorentzian approach. Conversely, the 7.7-μm band, for example, contains several recognizable subfeatures, and, indeed, there is no intrinsic reason that the emission spectrum of a family of PAHs would result in a Gaussian distribution of peak positions. Because the observed interstellar emission profiles are clearly not Gaussian, Lorentzian, or even symmetric—the 6.2-μm and 11.2-μm bands look anharmonic—these assumptions impose the presence of subfeatures that may not be real. Fortunately, extensive comparisons have shown that trends such as correlations among the relative strength of the different features are not affected by the particular method adopted (Smith et al. 2007, Galliano et al. 2008).

3. THE CHARACTERISTICS OF INTERSTELLAR POLYCYCLIC AROMATIC HYDROCARBONS

3.1. Polycyclic Aromatic Hydrocarbon Structures

PAHs compose a family of hydrocarbon molecules with C atoms arranged in a honeycomb structure of fused six-membered, aromatic rings with peripheral H atoms. The C atoms are bonded to each other or to an H atom (for peripheral C atoms) through three sigma bonds, resulting in a planar structure. The fourth electron of each C atom is in a *p* orbital sticking out of the plane. The *p* electrons on adjacent C atoms overlap to form π bonds and delocalized electron clouds

above and below the plane. This conjugation is the origin of the high stability of these types of species. Allamandola, Tielens & Barker (1989, their figure 1) illustrate molecular structures for some simple PAHs. Centrally condensed, compact PAHs such as coronene ($C_{24}H_{12}$) are, as a class, very stable because this structure allows complete electron delocalization and truly aromatic bonding between all adjacent C atoms. The radius of the disk of centrally condensed compact PAHs is given by $a \simeq 0.9\, N_C^{1/2}$ Å.

The distribution of hydrogens on the periphery of the PAHs is indicated by solo H atoms (no H atoms attached to adjacent C atoms), duos (two adjacent C atoms, each with an H atom), trios (three adjacent C atoms, each with an H atom), and quartets (four adjacent C atoms, each with an H atom). **Figure 7** shows some example molecular structures. Other functional groups such as methyl (-CH_3) can be substituted for hydrogen (substituted PAHs). Geballe et al. (1989, their figure 3) illustrate some typical examples of such functional groups. In dehydrogenated PAHs, some peripheral H atoms have been lost. Superhydrogenated PAHs (also called hydro-PAHs)—where some peripheral C atoms have two hydrogens, and thus an aliphatic character—have also been considered in an astrophysical context. Species that contain noncarbon ring atoms are called heterocycles. The planar structure of the PAHs facilitates stacking into so-called PAH clusters bonded by van der Waals forces (see Section 4.2.4).

3.2. Assignments

The well-known IR emission features at 3.3, 6.2, 7.7, 8.6, and 11.3 μm are characteristic of the stretching and bending vibrations of aromatic hydrocarbon materials (Allamandola, Tielens & Barker 1989) (**Figure 1*a***). The 3-μm region is characteristic of CH stretching modes, and the 3.3-μm band results from the CH stretching mode in aromatic species. Pure CC stretching modes generally fall between 6.1 and 6.5 μm, vibrations involving combinations of CC stretching and CH in-plane bending modes lie slightly longward (6.5–8.5 μm), and CH in-plane wagging modes give rise to bands in the 8.3–8.9-μm range. The 11–15-μm range is characteristic of CH out-of-plane bending modes. Longward of 15 μm, emission bands reflect in-plane and out-of-plane ring bending motions of the carbon skeleton; hence these modes are more molecule specific, particular to the longer wavelengths.

These assignments to specific modes of polycyclic aromatic materials are generally agreed upon and noncontroversial. There is more discussion, however, on the assignment of the weaker features. For example, the 3.4-μm band—which in a few spectra is as strong as the 3.3-μm feature—is indicative of an aliphatic CH stretching mode. This band may result from aliphatic groups attached as functional groups to the PAHs or from hydroPAHs in which the extra hydrogen bonded to some carbons has destroyed the aromatic character, led to ring puckering, and resulted in a shift in the peak frequency of the CH stretch (Schutte, Tielens & Allamandola 1993; Bernstein, Sandford & Allamandola 1996; Joblin et al. 1996; Sloan et al. 1997; Wagner, Kim & Saykally 2000). The presence of a feature at 6.9 μm in some spectra provides general support for the aliphatic interpretation. However, this 6.9-μm band could also be a (weak) CC mode; moreover, a strong 3.4-μm band does not always go hand in hand with a strong 6.9-μm band. The interpretation in terms of hydroPAHs is controversial because of the limited stability of such species (see Section 5.4.3) (Le Page, Snow & Bierbaum 2003).

3.3. Aromaticity and the Infrared Emission Features

The Short Wavelength Spectrometer (SWS) on ISO and, to a lesser extent, the IRS on Spitzer have provided complete coverage of the interstellar IR emission band spectrum. This spectral

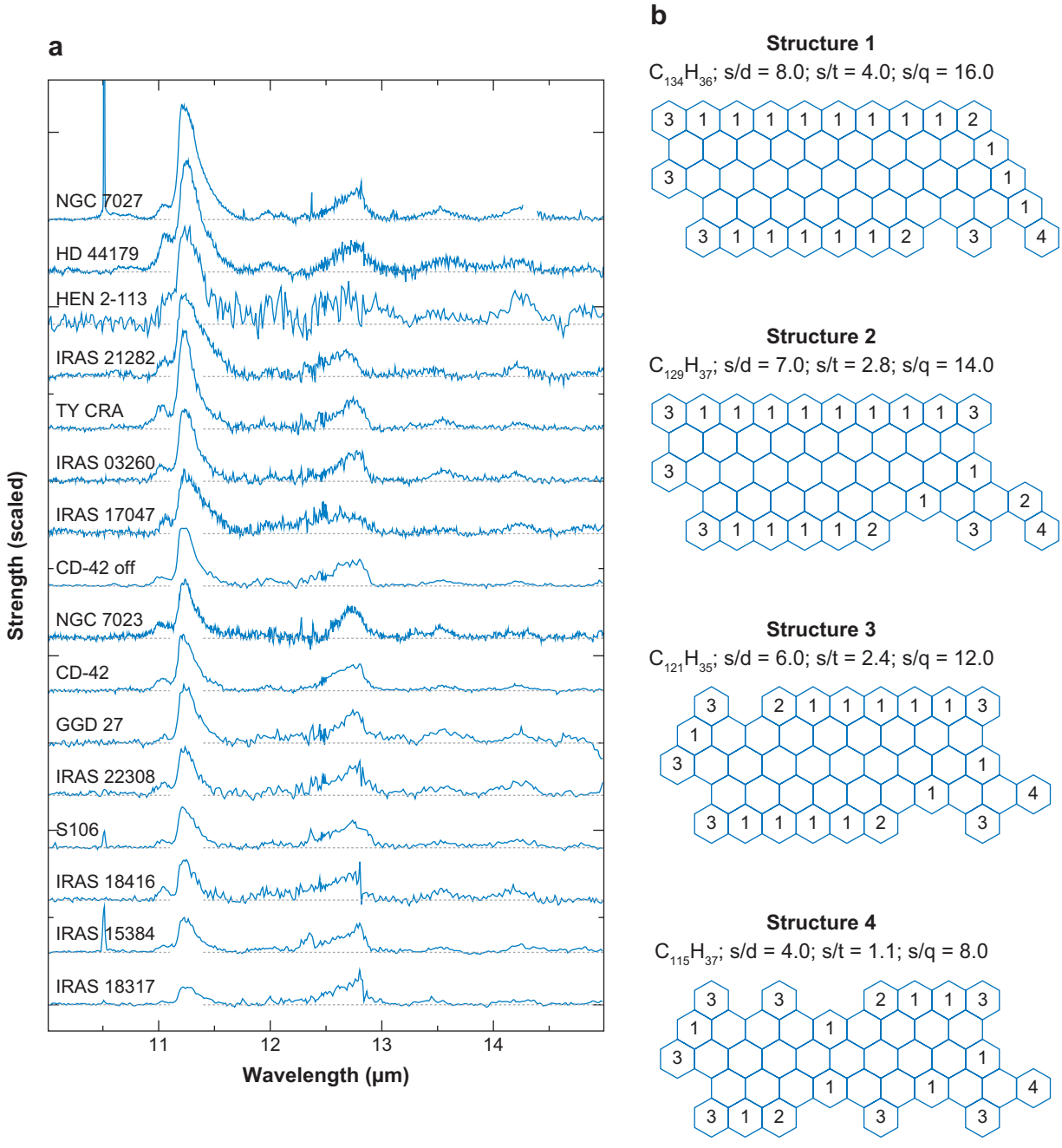

Figure 7

(*a*) An overview of the observed feature variations in the out-of-plane bending region. The Infrared Space Observatory–Short Wavelength Spectrometer spectra are continuum subtracted, scaled to have the same integrated intensity in the 12.7-μm feature, and arranged in order of decreasing 11.2-μm strength: (*from top to bottom*) planetary nebulae, Herbig stars, reflection nebulae, and HII regions. (*b*) Examples of molecular structures simultaneously satisfying the structural constraints set by the observed feature strength ratios of the number of solo (s), duo (d), and trio (t) modes for different interstellar regions. Solo modes are associated with long straight molecular edges, whereas duo and trio modes correspond to corners. Figure taken from Hony et al. 2001.

Table 1 The overwhelming aromatic nature of the unidentified infrared bands

Functional group	λ (μm)	Fraction[a]
Aromatic H	3.3	1
Aliphatic CH_3	3.40	0.02
Aliphatic deuterium CH_2D	4.65	0.02
Hydroxyl (OH)	2.77	<0.002
Amine (NH_2)	2.88–2.95	<0.01
Aldehydic (HCO)	5.9	0.006 (?)
Nitrile (C≡N)	4.48	<0.01 (?)
N substituted in the ring structure[b]	6.2	0.04 (?)
Acetylenic (C≡CH)	3.03	<0.003

[a]Fraction relative to aromatic hydrogen.
[b]Fraction relative to carbon.

coverage has allowed a detailed analysis of the molecular structure of the carriers. Of particular interest is the fractional abundance of various side groups on the emitting PAHs (**Table 1**). The overwhelming majority of the peripheral sites of the aromatic carrier of the IR emission features contain aromatic hydrogen, with a minute amount of aliphatic CH_3 groups and possibly some aldehydic groups (HCO). Clearly, the carrier of IR emission features does not consist of aromatic units bound by aliphatic chains in a three-dimensional, coal-like, or hydrogenated amorphous carbon–like structure. In principle, the spectroscopic evidence still allows a 50 C-atom carrier comprising PAH units bonded together in a three-dimensional network by physical van der Waals forces. However, two small PAHs, such as coronene ($C_{24}H_{12}$), are bonded by only ~1.3 eV, and FUV photon absorption rapidly breaks down such a cluster (Rapacioli et al. 2006). There are some exceptional post-AGB sources with spectra that reveal abundant aliphatic hydrocarbon groups, but (apparently) these do not survive the harsher conditions of the ISM (see Section 5.4.1).

A band at 4.65 μm has been detected at the 4.4 σ level in the ISO-SWS spectra of the Orion Bar and M17 (Peeters et al. 2004a). This position is characteristic of the CD stretch in deuterated aliphatic hydrocarbons. The observed strength of this band implies that aliphatic deuterium is about as abundant as aliphatic hydrogen. Curiously, there is little evidence for the presence of aromatic deuterium with a limit of aromatic D/H < 0.05. Hence, if this interpretation is correct, deuterium fractionation of PAHs must be highly specific. These aliphatic groups likely result from local processing, and the high deuterium fractionation may just reflect that H_2 is self-shielding in PDRs and HD is not; hence the local, gas-phase atomic D/H abundance—which drives the fractionation—is high. The gas-phase D/H abundance ratio varies considerably in the local ISM, which has been attributed to deuterium locked up in dust and/or PAHs (Linsky et al. 2006). These observations show that PAHs are not an important carrier of atomic deuterium. We note that, likewise, there is no evidence for abundant aliphatic CD modes (the analog of the 3.4-μm band) in the absorption spectrum of interstellar dust (Whittet et al. 1997).

3.4. Abundances

The abundance of C, f_c locked up in interstellar PAHs can be derived relatively simply from observations by realizing that the total IR emission flux is equal to the total UV flux absorbed. The ratio of the flux in IR emission features to the far-IR flux is then equal to the UV flux absorbed by PAHs as compared with that absorbed by dust. Adopting standard dust parameters

Table 2 Abundances of the carriers of infrared (IR) emission components

Carrier	IR emission component	N_c	a (Å)	f_C[a] (ppm)[b]
PAHs	IR emission features	20–100	4–10[c]	14
PAH clusters	Plateaus	100–1000	10–20	8
Very small grains	25-μm cirrus	10^3–10^4	20–30	7
Small grains	60-μm cirrus	$\sim 10^5$	50	16
Classical grains	$\lambda > 100$ μm		>100	35[d]?
C chains[e]	IR emission	>3		$<3 \times 10^{-1}$
C_{60}[f]	Far-red absorption bands			2

PAH, polycyclic aromatic hydrocarbon.
[a]Abundance of C locked up in these species relative to H nuclei.
[b]Parts per million.
[c]Size corresponds to disk rather than sphere.
[d]The abundance of C locked up in dust grains is uncertain.
[e]Abundance of carbon chains estimated from upper limits on their IR emission. For comparison, the measured fraction of C locked up carbon chains in dense clouds is 8×10^{-2} ppm.
[f]Two far-red absorption bands have been attributed to C_{60}. Upper limits on IR emission bands due to this molecule are consistent with this estimate.

and measured UV-absorption cross sections for PAHs, this yields the fraction of C locked up in PAHs (Allamandola, Tielens & Barker 1989).

Table 2 gives typical values for the abundance of PAHs in bright PDRs. The fraction of the elemental C locked up in PAHs is $\sim 3.5 \times 10^{-2}$. This simple estimate is similar to the results obtained through detailed modeling of the spectral energy distribution of the Milky Way (see Section 3.9). With a typical size of 50 C atoms, the PAH abundance is $\sim 3 \times 10^{-7}$ relative to hydrogen nuclei. Similar fractions of the carbon are locked up in PAH clusters of ~400 C atoms, which carry the plateau emission underlying the IR emission features, and in 20–30-Å very small grains, which are responsible for the 25-μm cirrus. The abundance of small grains responsible for the fluctuating part of the 60-μm cirrus is slightly larger. These PAH abundances are based on observations of well-developed PDRs such as the Orion Bar and the reflection nebula NGC 2023. The PAH over far-IR ratios for many HII regions are an order of magnitude lower, possibly because of a reduced PAH abundance or because much of the stellar FUV flux is absorbed by dust in the HII region and does not reach the PAHs in the PDR (see Section 7.2) (Peeters, Spoon & Tielens 2004**)**. PAH bands are also notably weak in the spectra of Herbig AeBe and T Tauri stars (see Section 7.1), possibly reflecting low PAH abundances in their circumstellar disks (Manske & Henning 1999, Geers 2007).

The available spectra can also be perused for the presence of other classes of molecules. Large hydrocarbon chains of course are of particular interest in view of their presence in molecular clouds and their likely connection to the diffuse interstellar band (DIB) problem (see Section 4.3.1) (Maier, Walker & Bohlender 2004; Maier et al. 2006). Acetylenic carbon chains absorb typically 1800–2100 cm^{-1} (4.8–5.5 μm) (Allamandola et al. 1999). SWS spectra of bright PDRs associated with HII regions or PNe do not show a distinct feature at these wavelengths; hence the abundance of such species is small compared with that of the PAHs in these regions. Unfortunately, neither ISOPHOT-S, ISOCAM-CVF, Spitzer IRS, nor the Japanese Infrared Telescope in Space covered this wavelength region, but an upper limit to the abundance of carbon chains in the diffuse ISM can be determined by combining ISOCAM and DIRBE data. Comparing these data, the emission in the M band, and thus in carbon chain vibrational modes, is less than 0.02 of that in the PAH modes, which is then also the ratio of the UV absorbed by these species. For these molecules, the

UV absorption is dominated by their π-electron system with similar intrinsic strength per C atom to that of PAHs, which results in the values given in **Table 2** for carbon chains in the diffuse ISM. As a corollary, if carbon chains—or actually any DIB carrier apart from the PAHs—are indeed the carriers of the DIBs, the oscillator strength of the transitions involved has to be very large.

3.5. CH Out-of-Plane Bending Modes and Polycyclic Aromatic Hydrocarbon Molecular Structure

The 11–15-μm region of the spectrum is rich in detail and contains bands at 11.0, 11.3, 11.9, 12.8, 13.6, 14.2, and 14.8 μm (**Figure 7**). Extensive laboratory studies have shown that the peak wavelength of the CH out-of-plane bending mode depends sensitively on the number of adjacent peripheral C atoms bonded to an H atom (Hudgins & Allamandola 1999b, Hony et al. 2001). Although the details depend slightly on the carrier's charge state, the 11.2-μm feature can be safely ascribed to lone CH groups, and the 12.7-μm feature belongs to trios with possibly a contribution by duos. In terms of molecular structure, lone CH groups are part of long straight edges, whereas duos and trios are characteristic of corners. Variations in the relative strength of the 11.2-μm to the 12.7-μm feature thus indicate variations in the molecular structure of the emitting PAHs (**Figure 7**). Recent density functional theory (DFT) calculations (Bauschlicher, Peeters & Allamandola 2008) have revealed that, if large compact PAHs dominate, the 12.8-μm band results from duos rather than trios, but the overall conclusion still stands: Circumstellar PAHs associated with PNe are characterized by compact molecular structures, whereas interstellar PAHs have more corners, either because they are (on average) much smaller or because they have more highly irregular, corrugated edge structures. These differences have been attributed to photoprocessing in the harsh environment of the ISM.

3.6. The Degree of Ionization

The relative strength of the CH and CC modes varies substantially from source to source and between sources (see Section 2.2.1). These variations have been attributed to the effect of ionization on the intrinsic strength of the CC versus the CH modes (see Section 4.2.1). Hence, the 6.2-μm to 11.2-μm ratio provides a good measure of the ionization balance of the emitting PAHs. The PAH charge depends on the ratio of the ionization rate to the recombination rate [i.e., $G_o T^{0.5}/n_e$, where G_o is the intensity of the ambient radiation field in units of the Habing field (1.2×10^{-4} erg cm^{-2} s^{-1} sr^{-1}), T is the gas temperature, and n_e is the electron density] (Bakes & Tielens 1994). As a result, the emitted spectrum depends on the local physical conditions, and the observed variations in the 3.3-μm, 11.3-μm to 6.2-μm, 7.7-μm ratio (**Figures 3** and **6**) reflect variations in physical conditions (Hony et al. 2001, Galliano et al. 2008, Flagey et al. 2006, Berné et al. 2007). The observed CC/CH ratio can be linked to the local physical conditions for a few PDRs that have been well studied in diagnostic atomic fine-structure lines and molecular rotational lines (**Figure 8**) (Galliano et al. 2008). This observational relation has the potential to turn PAH observations into quantitative probes of the local physical conditions.

Finally, we note that the 11.0-μm band has been attributed to the CH out-of-plane bending mode of lone hydrogen groups in PAH cations. Hence, the ratio of the 11.0- to 11.2-μm bands is (in a convoluted way) a measure of the degree of ionization of PAHs as well. Likewise, the 18.9-μm band may result from doubly charged PAHs (see Section 3.8), providing yet another handle on the PAH charge distribution.

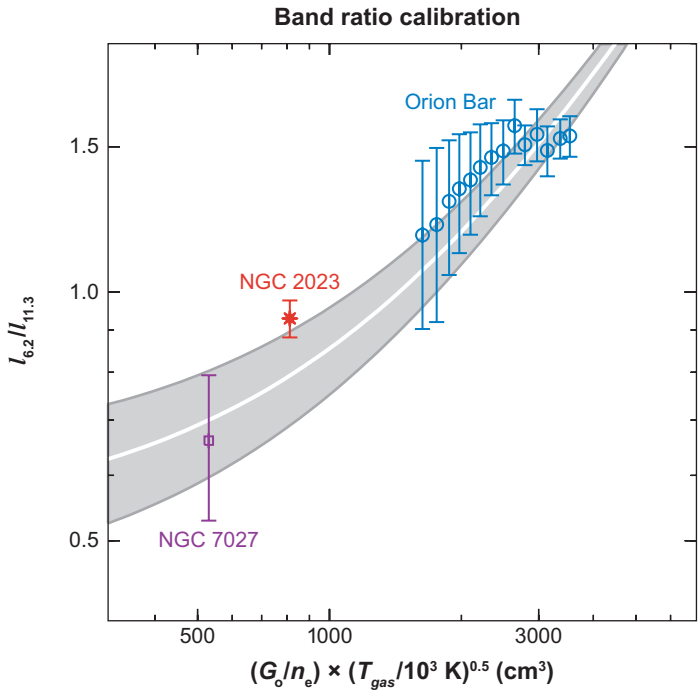

Figure 8

For a few well-studied photodissociation regions, the ratio of the 6.2-μm to 11.2-μm bands can be determined as a function of the ionization parameter, $G_o T^{1/2}/n_e$. The degree of ionization of polycyclic aromatic hydrocarbons increases to the right as either the strength of the ionizing ultraviolet field, G_o, increases or the electron density, n_e, decreases. The temperature, T, enters through the velocity dependence of the Coulomb focusing factor. Figure taken from Galliano et al. 2008.

3.7. Spectral Variations of the CC Modes

The observed variations in the 6.2-μm peak position (see Section 2.2.2) have been attributed to the effect of nitrogen substitution (see Section 4.2.3), and the full range of observed peak positions can be explained by moving the substituted nitrogen more to the interior of the aromatic ring system. Alternatively, this shift may reflect clustering of PAHs either with each other or with metal atoms (see Sections 4.2.3 and 4.2.4), and there is some support for this in the observed spatial distributions of the principal components deduced for the reflection nebula NGC 7023 (see Section 2.2.3 and **Figure 6**) (Rapacioli, Joblin & Boissel 2005). However, there is presently little experimental or quantum chemical data on such systems, and this hypothesis has not been critically examined.

3.8. Emission Features in the 15–20-μm Range

ISO-SWS already revealed a number of emission features in the 15–20-μm region that typically blend in a plateau (Moutou et al. 2000, Van Kerckhoven et al. 2000). However, it took the smaller beam size and higher sensitivity of Spitzer IRS to fully appreciate the spectral structure in this wavelength region (Werner et al. 2004), revealing discrete bands at 15.9, 16.4, 17.4, 17.8, and 18.9 μm (**Figure 9**) (Sellgren, Uchida & Werner 2007). The strength of the strongest band at 16.4 μm

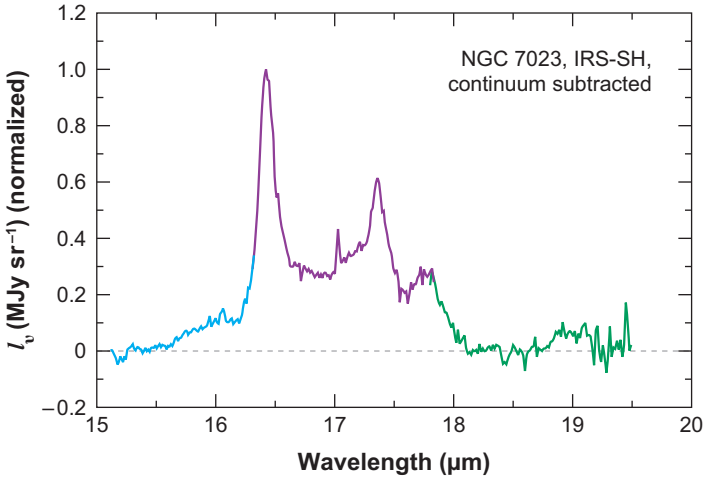

Figure 9

The high-resolution 15–20-μm spectrum of the reflection nebula NGC 7023, obtained with the Spitzer IRS (Sellgren, Uchida & Werner 2007), reveals a wealth of spectral detail. The different spectral orders are indicated with different colors.

follows that of IR emission features well. Similarly, in a sample of galaxies, the whole 17-μm complexes follow the 11.2-μm band well (Smith et al. 2007).

In principle, this spectral region has great potential for the identification of specific PAH molecules. In the mid-IR, the vibrational spectrum reflects nearest-neighbor vibrations. As a result, IR modes occur at very similar wavelengths. In contrast, at longer wavelengths, emission results from in-plane and out-of-plane ring bending modes of the carbon skeleton, which are more molecule specific. These PAH modes have been studied in the laboratory by Moutou, Leger & D'Hendecourt (1996) and theoretically by Bauschlicher (2002). The IR spectrum of the PAH collection studied by Moutou, Leger & D'Hendecourt (1996) shows absorption bands throughout this wavelength region, with distinct features at 16.2 and 18.2 μm, at which 20% and 50% of the PAHs considered show a band, respectively. Typically, a collection of spectra from the experimental or theoretical database results in a broad emission plateau from ∼16 to 19 μm, with some spectral substructure whose detail depends on the selected mixture (Van Kerckhoven et al. 2000, Peeters et al. 2004b). Overall, the presence of a limited number of bands in the observed spectra, coupled with the sensitivity of these bands to the larger molecular structure, implies that the emitting interstellar PAH family is dominated by a few classes of PAHs with well-defined molecular structures. These classes likely include the large, compact, highly symmetric PAHs, but this has not been investigated in detail.

Sellgren, Uchida & Werner (2007) note that—unlike the other bands in this wavelength region—the 18.9-μm feature is localized directly around the illuminating star in NGC 7023 (compare with **Figure 6**). Hence, this band may be characteristic of highly ionized PAHs (e.g., PAH^{2+} if $N_C \simeq 50$ or even PAH^{3+} if $N_c \sim 100$ C atoms). This would be exciting because, together with the 11.2-μm and 6.2/7.7-μm bands, variations in the degree of ionization can be traced in detail, and this has obvious implications for studies of the photoelectric heating of the gas, as well as the influence of PAHs on the ionization balance of the gas (see Section 6.2). However, the identification of the 18.9-μm band with a more exotic but stable species (e.g., neutral or cationic C_{60}) has also been suggested (Sellgren, Uchida & Werner 2007).

3.9. Fitting the Observed Spectra

Detailed models for the global IR emission characteristics of the ISM have been developed (Desert, Boulanger & Puget 1990; Draine & Li 2001; Galliano, Dwek & Chanial 2008). These models assume, commonly, that the size distribution of interstellar dust extends smoothly into the molecular domain, and they employ idealized, intrinsic properties of the interstellar PAH family. These properties, derived from the extensive laboratory and quantum chemical studies, include dependencies on PAH size and (often) PAH charge state. However, the details of the intrinsic emission spectrum (e.g., number of IR active modes, peak position, and width) are arbitrarily set to values that mimic the observed characteristics. Fitting the observed spectra boils down then to adjusting the PAH abundance until the observed PAH-to-far-IR continuum ratio is met. The PAH cation/neutral ratio also enters in these fits but can be adjusted through G_o/n. In a general sense, these models link global descriptions of dust properties over a wide range of sizes to a heating/cooling prescription and—with a simple parametric description of the galaxy characterizing a distribution of G_o and G_o/n_e, and the shape of the incident radiation field—calculate the resulting IR emission spectrum (Draine et al. 2007; Galliano, Dwek & Chanial 2008).

Draine & Li (2007) have made extensive fits to spectral energy distributions that require small tweaks to earlier dust models. ISO data on galaxies have been analyzed and interpreted by Galliano et al. (2008). The Spitzer SINGS survey has provided a wealth of data on the PAH and dust emission characteristics of galaxies. Draine et al. (2007) have analyzed this data. The results (**Figure 10**) show that typically the fraction of the mass locked up in PAHs relative to the total dust mass, q_{PAH}, is approximately 4×10^{-2}. This is similar to the value in the Milky Way (see Section 3.4). Low-metallicity galaxies ($A_O < 8.1$, 1/4 solar), however, are characterized by much

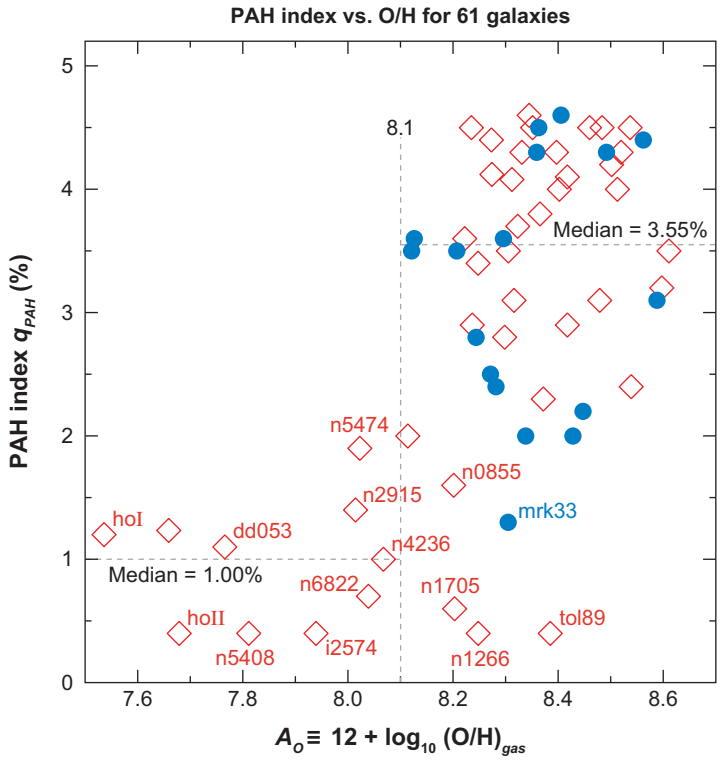

Figure 10

Polycyclic aromatic hydrocarbon (PAH) mass abundance relative to the total dust mass, q_{PAH}, as a function of galaxy metallicity. Filled circles have submillimeter data, and open diamonds do not. Figure taken from Draine et al. 2007.

lower PAH abundances ($q_{PAH} \simeq 10^{-2}$) (Engelbracht et al. 2005; Madden et al. 2006; Wu et al. 2006; Draine et al. 2007; Galliano, Dwek & Chanial 2008). In addition, analysis of the SINGS sample has revealed that, on a global scale, most of the dust-continuum emission originates from the diffuse ISM characterized by low values of the incident FUV radiation field ($G_o \simeq 3$), and only ~10% comes from PDRs associated with regions of massive star formation ($G_o > 10^2$) (Draine et al. 2007). This is likely true for IR emission features as well, which is perhaps not surprising because the stellar luminosity is dominated by mid-B stars, which wander much further from their natal molecular clouds than O stars (see Peeters, Spoon & Tielens 2004).

A different and complementary approach has been taken by Bakes et al. (2001; Bakes, Tielens & Bauschlicher 2001) and by J. Cami and coworkers (manuscript in preparation), which focuses on fitting observed emission spectra in detail to derive the composition and characteristics of the interstellar PAH family. These studies have taken the intrinsic properties of actual molecules as the basis of their modeling efforts. In particular, this includes the actual peak positions of the IR active modes—from laboratory or quantum chemical studies—as well as ionization potentials. UV absorption rates are idealized again (but that is less critical). Bakes et al.'s studies focus on a limited number of species within specific classes of PAHs, whereas Cami et al.'s study includes the full available, theoretically calculated, NASA Ames PAH spectral database. Good fits (**Figure 11**)

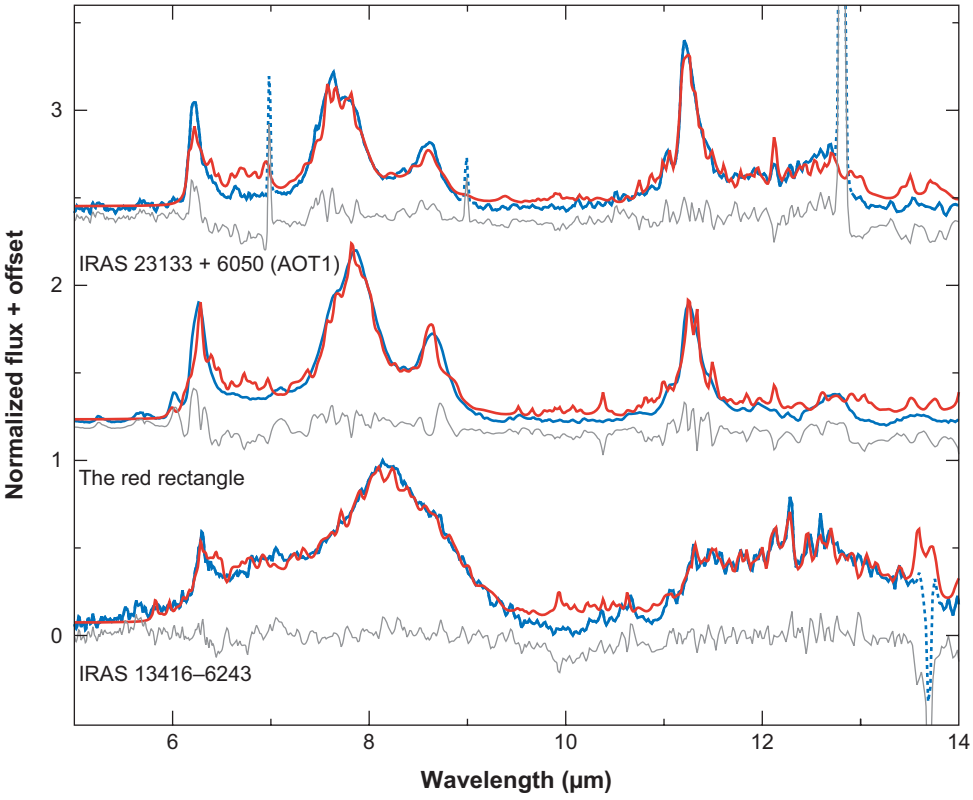

Figure 11

Fits (*blue*) to the observed (*red*) 5–14-μm spectrum of characteristic representatives of class A, B, and C sources (*red*; see **Figure 4**). Residuals are shown as thin gray lines. Measured or calculated intrinsic emission properties of the specific polycyclic aromatic hydrocarbons present in the NASA Ames database have been used. Figure provided by J. Cami.

can be obtained for all three classes of interstellar spectra (A, B, and C; see Section 2.2.2). Of course, in evaluating these fits, the inherent uncertainties in the calculated PAH spectral data should be kept in mind (see Section 4). Comparison of the families required for the different classes substantially confirms the conclusions on the molecular structures and degree of ionization involved derived before and discussed above: For class A, emission in the 6–9-μm range is due to cations with a large contribution of N-substituted PAHs to the 6.2-μm band. For class B and C, N-substituted PAHs do not contribute appreciably. Small and large PAHs contribute about equally to this wavelength range. Neutral PAHs dominate the 11–15-μm range for all classes. J. Cami et al. (manuscript in preparation) show that, for class A and B, large PAHs dominate this wavelength range, whereas for class C, small PAHs take over. As future dedicated experimental or theoretical studies address the caveats, as well as the pitfalls, discussed in Section 4, this type of analysis will provide a powerful tool to direct research in this area, for example, in terms of identifying relevant molecular structures in an unbiased way. For now, I interpret the available evidence to point toward a PAH family that comprises a surprisingly limited number of compact, highly symmetric, large PAHs in the ISM, which is modified in circumstellar environments by a rich chemistry.

4. POLYCYCLIC AROMATIC HYDROCARBON SPECTROSCOPY

Experimental studies of the intrinsic spectra of gaseous PAHs are not straightforward, given the low vapor pressure of PAHs, which makes it difficult to keep them in the gas phase. In addition, space-charge and reactivity considerations limit the concentration of PAH ions and radicals. Conversely, in the solid state, individual PAHs are not isolated and may interact strongly with each other or with the surrounding medium. Nevertheless, much progress has been made over the past decade in determining the intrinsic spectral properties of PAH molecules owing to the dedicated efforts of a number of laboratory groups using a variety of complementary experimental techniques. These studies have benefited much from the guidance of theoretical calculations using DFT. Each technique has its advantages and disadvantages, and Oomens et al. (2003) have critically reviewed them. These studies have focused on measuring the IR characteristics of PAH cations because of early speculation that ionization might have important effects on the spectra (Allamandola, Tielens & Barker 1985), which was underpinned by theoretical calculations (de Frees et al. 1993, Langhoff 1996). **Figure 12** compares the spectra obtained for two small PAH in neutral and cationic forms using these different techniques. The experimental and quantum chemical data have been made available through dedicated websites (**http://www.astrochem.org/pahdata** and **http://astrochemistry.ca.astro.it/database/**).

4.1. Techniques

Here, we review the different techniques that have been used to determine the intrinsic spectral characteristics of PAH species and compare and contrast their (dis)advantages.

4.1.1. Matrix isolation spectroscopy. Matrix isolation spectroscopy (MIS) is a well-established technique that isolates reactive or transient species in an inert matrix (e.g., Ne, Ar). These studies mix neutral parent species with noble gas species and deposit them on a cold finger at 10 K or less. For neutral species, interaction of a PAH with the matrix is small. Irradiation of the sample by an FUV light produces cations, and their absorption spectrum can be measured in the IR, visible, and UV using standard spectrometers. However, the ionization efficiency is not high, and confusion with bands owing to the neutral parent molecule (e.g., the C-H stretching region) is always a problem. Additionally, the photolysis may produce other species (e.g., dehydrogenated

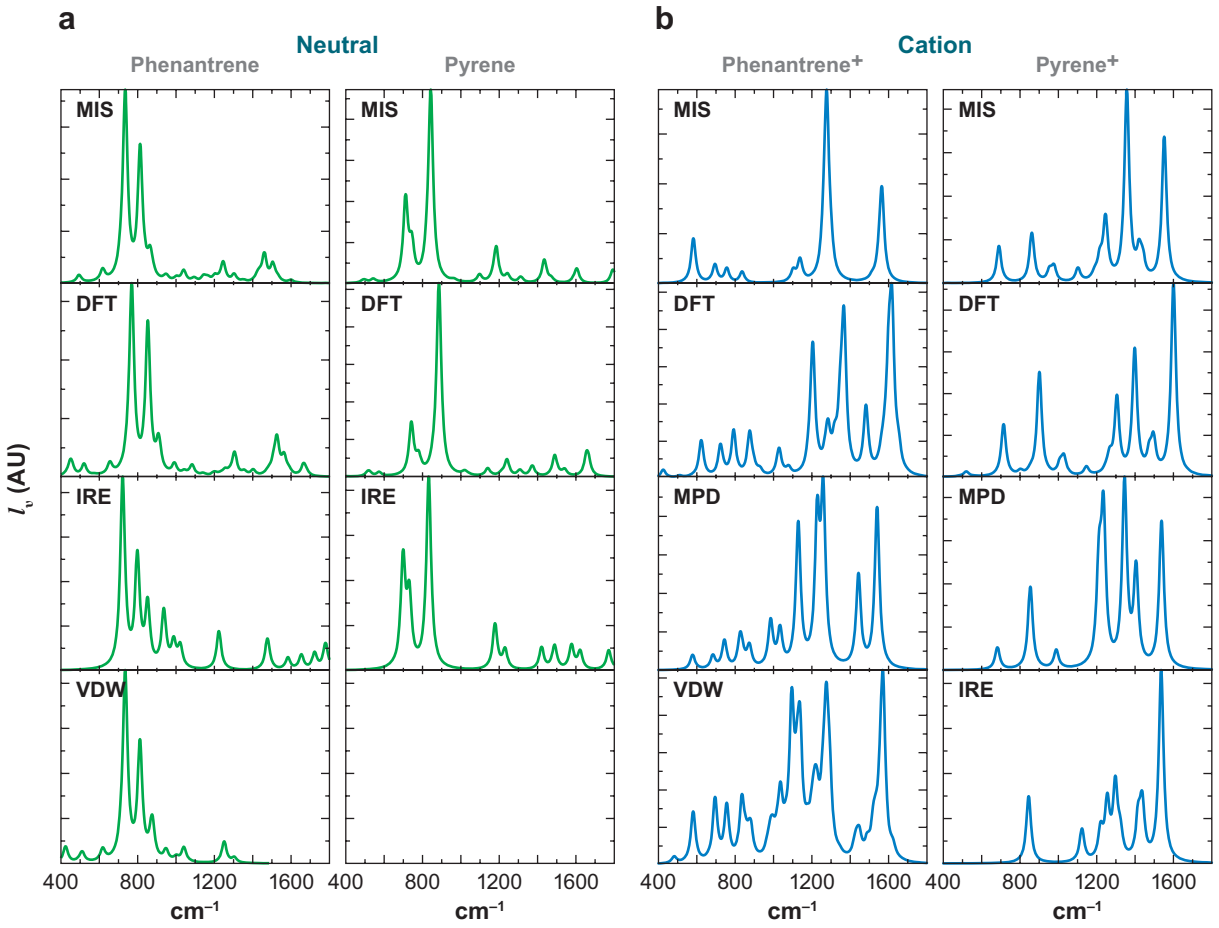

Figure 12

A comparison of the neutral (*a*) and cation (*b*) spectra of the polycyclic aromatic hydrocarbons phenanthrene ($C_{14}H_{10}$) and pyrene ($C_{16}H_{10}$) obtained using different techniques: matrix isolation spectroscopy (MIS), density functional theory (DFT), infrared emission (IRE), multiphoton dissociation (MPD), and van der Waals clusters (VDW). Note that the different techniques do not always cover the same frequency range.

radicals). Assignments of bands to the cationic species can be facilitated by further experiments using mixtures doped with well-known electron acceptors (e.g., CCl_4). Also, small PAHs have no (electronic) absorption bands in the visible. Hence, the correlation of the growth of IR bands with visible electronic transitions of cations (where confusion is no issue) or with UV dose can be helpful in this respect. Ion-matrix interactions are much more important than neutral-matrix interactions, giving rise to larger shifts, wider profiles, and larger intensity changes. The advantage of this technique is the relative ease with which different species can be studied, and a large sample of PAHs has been studied over the past 15 years (Szczepanski & Vala 1993; Moutou, Leger & D'Hendecourt 1996; Hudgins & Allamandola 1999a,b).

4.1.2. Multiphoton dissociation techniques. Multiphoton dissociation (MPD) techniques produce ions in the gas phase through photoionization with an FUV laser. These ions are stored in an

ion trap, which can be manipulated to reject other species to avoid confusion. Space-charge considerations hamper the use of conventional spectroscopic techniques to measure the absorption properties of the ion. Instead, an intense IR-tunable, pulsed, free-electron laser is used. When the wavelength of the laser is in resonance with an absorption band, the trapped species can rapidly absorb a large number of photons, and when it is highly excited, dissociation results. The number of fragments produced and initial cations remaining can be readily measured using time-of-flight ion-mass spectrometry. Mass spectrometry is a sensitive technique, and even small amounts can be reliably measured. Frequency scanning of the IR laser then results in the equivalent of an IR spectrum. Although this technique is straightforward, it does require access to a free-electron IR laser, and only a few are available worldwide. Besides the specialized equipment, this technique also has some experimental drawbacks. In particular, the IR photon energy (0.05 eV) is much less than the typical internal energy required for dissociation (~10 eV). Hence, many photons have to be absorbed before dissociation occurs. The peak position (e.g., red shift) and band strength may be adversely affected by anharmonicity effects, which are inherent to highly excited species; indeed large anharmonicities may even shift the absorption band outside the pumping frequency before dissociation occurs. Furthermore, the spectral resolution (5 cm^{-1}) of this technique is limited by the short pulse duration (~1 ps) of the laser. This technique also has a number of clear advantages: The species are in the gas phase, not in a matrix; specific ions are readily isolated; it is extremely sensitive and relatively simple; and—turning a vice into a virtue—it also allows the study of the mode's anharmonicity. Presently, the Dutch laser FELIX has been used to measure a number of small PAH cations (Oomens et al. 2000, 2001, 2003), and the French laser CLIO has measured protonated naphthalene (Lorenz et al. 2007).

4.1.3. van der Waals clusters. The dissociation of van der Waals clusters is a variant of the MPD technique. In this case, a cluster of the neutral PAH with a loosely bound, noble gas atom (e.g., Ar) is formed in the supersonic expansion of a molecular beam. The neutral cluster is then ionized with a double-resonant ionization scheme that leaves the ionic cluster just above the ionization potential but internally cold. The absorption of a single IR photon dissociates the cluster, and the resulting bare PAH cation can be counted using a time-of-flight mass spectrometer. Again, this technique requires a tunable intense IR laser for an absorption spectrum and hence limits the spectral resolution to approximately 5 cm^{-1}. Also, the preparation of the species is molecule specific. The shift induced by the complexed noble atom has to be established but turns out to be small (1 cm^{-1}) compared to the spectral resolution. Some other subtle spectral effects can also occur. Therefore, this technique is more involved than the two listed above. However, it does overcome the problem of the anharmonicity associated with the MPD studies. Presently, only the IR absorption spectra of the naphthalene and phenanthrene cations have been measured this way (Piest, von Helden & Meijer 1999).

4.1.4. Infrared emission. The most direct test of the interstellar PAH hypothesis is to measure the IR emission (IRE) spectrum of a highly excited PAH species in the gas phase. For neutral PAHs, this has been done in the 3-μm region following excitation by UV absorption or heating in an oven (Kim & Saykally 2002). Because of the high background, this method becomes challenging at longer wavelengths. Nevertheless, for a few neutral PAHs, this IR emission technique has been extended to longer wavelengths using a cryogenically cooled IR spectrometer capable of counting single IR photons (Schlemmer et al. 1994, Cook et al. 1998). Whereas this technique is already involved for neutral PAHs, studying the IR spectra of PAH cations is particularly daunting because of space-charge limitations. However, the Saykally group (Kim, Wagner & Saykally 2001; Kim & Saykally 2002) in Berkeley has succeeded in measuring the IR spectra of a few PAH cations in the

gas phase that were ionized (and excited) by electron impacts. This technique measures precisely what is needed, the IR emission spectrum of a highly vibrationally excited PAH cation in the gas phase (a feat that cannot be lauded enough). However, this technique is difficult and is limited to relatively small species. Also, the internal energy of the emitting species is difficult to quantify (and the exact peak position depends on the internal energy). Moreover, this technique requires the use of a unique IR spectrometer that is presently (and unwisely) not funded for astronomical studies. Hence, only the pyrene cation and some of its derivatives have been studied.

4.1.5. Density functional theory. Although Hartree-Fock ab initio techniques have been used to calculate the spectroscopic properties of PAHs (de Frees et al. 1993; Pauzat, Talbi & Ellinger 1997), for large molecules these techniques generally do not reach the level of accuracy required. For PAHs containing dozens of electrons, the semiempirical DFT (density functional theory) provides an attractive alternative that has been instrumental in guiding the interpretation and analysis of experimental studies (Langhoff 1996, Bauschlicher & Bakes 2000, Bauschlicher 2002). The ease and speed of the calculation must be balanced with the accuracy of the results. Typically, these calculations are done using the B3LYP modification of the Becke hybrid functional and the 4-31 G Gaussian basis to expand the molecular orbitals. Extensive calculations have been made to assess systematic effects associated with the basis set, and generally the resulting frequencies are scaled by a factor of 0.96 derived this way (Langhoff 1996). The influence of other systematic effects is more difficult to evaluate (e.g., the presence of low-lying electronic states may introduce erroneous results). One drawback is that only fundamental modes are calculated, and the many weak features due to combination bands or overtones are generally not included. DFT calculations have some clear advantages. A large number of similar species can easily be calculated and systematic trends investigated (e.g., the effects of symmetry and substitution). Also, whereas experimental studies are hampered by the low vapor pressure of large PAHs, with current computer capabilities, it is already feasible to calculate species containing up to ~130 C atoms, and Moore's law is on our side. It is also possible to study higher charge states, which have not yet been studied in the laboratory but are likely to be astronomically highly relevant. Finally, this method allows a detailed characterization of the absorption features (e.g., which atoms are involved in the vibrations), which aids in the interpretation of any observed trends. A large number of species have been calculated this way (Langhoff 1996; Bauschlicher & Bakes 2000; Bauschlicher 2002; Malloci, Joblin & Mulas 2007b; Bauschlicher, Peeters & Allamandola 2008).

4.1.6. Evaluation of the different techniques. For the neutrals, the comparison of the results obtained using different techniques is encouraging (**Figure 12**). Indeed, the overall pattern of absorption modes is very similar. All techniques show strong CH out-of-plane bending modes and weak CC stretching modes. Moreover, peak positions and relative intensities compare really well. In a detailed analysis of the CH stretching region (Huneycutt et al. 2004), comparison of jet-cooled IR cavity ringdown absorption spectra of small, neutral PAHs in the gas phase with MIS results reveal small matrix shifts (~3 cm^{-1}) and matrix broadening effects (up to an 80% increase). Similar shifts are apparent in a comparison of the gas-phase data with DFT calculations. The most important effect seems to be differences in relative intensity—both with the MIS and DFT results—which can conspire to give the resulting spectra a somewhat different appearance, including an overall peak position that is shifted (up to 10 cm^{-1}). For the other techniques, there is a small difference in peak position between the DFT results and the MIS and infrared emission measurements (**Figure 12**). The former may reflect matrix shifts, as well as an apparent shift introduced by differences in relative intensities of several modes contributing to the same band.

The latter may result from anharmonicity shifts for highly vibrationally excited species. Taking these small caveats into account, neutral spectra can be reliably compared with interstellar spectra.

For the ions, the overall comparison among the different techniques is also encouraging in terms of patterns and relative intensities (**Figure 12**). In this case, all techniques show strong CC stretching modes and relatively weak CH out-of-plane bending modes. However, the detailed comparison for the ions seems to be less favorable than for the neutrals. The IRE and DFT results for pyrene$^+$ agree reasonably well, given that there is an inherent anharmonic shift in the infrared emission peak positions. In contrast, the MPD results differ considerably in the relative intensity of the modes. Detailed analysis of the MPD data, using experimentally measured anharmonic shifts, shows that this likely reflects anharmonicity effects. Likewise, and not surprisingly, the relative band strength for cations seems to be affected by matrix effects in the MIS spectra. The difference between the van der Waals clusters and the DFT spectrum of phenanthrene$^+$ has been attributed to vibronic coupling of the vibrational states in the ground electronic state with those in the first excited electronic state. The Born-Oppenheimer approximation—used in the DFT calculations—does not fare well when vibronic coupling is involved. For phenanthrene$^+$ too, the MPD results seem to be noticeably affected by anharmonic effects, whereas the relative intensities seem to be affected by matrix effects in the MIS spectra. For cations, the DFT spectra are the most reliable, except when low-lying electronic states are present. Overall, global trends can be trusted, but care should be taken when comparing cationic spectra with measured interstellar spectra in detail.

4.2. Intrinsic Spectral Characteristics of Polycyclic Aromatic Hydrocarbons

The various techniques outlined above have been used to study systematically the IR emission characteristics of a large variety of species. Here, we review the effects of a number of key factors driving spectral variation.

4.2.1. Ionization. The charge state has a remarkable effect on the intrinsic IR spectra of PAHs. Whereas peak positions can shift somewhat, the intrinsic strength of modes is much affected. In particular, the strength of modes involving CC stretching vibrations can increase manifold upon ionization, whereas the CH stretching and, to a lesser extent, the out-of-plane bending vibrations decrease in strength. **Figure 13** compares the calculated/measured IR absorption cross sections for a family of PAHs in neutral and cationic states. This figure is based upon spectra of small ($<$50 C atoms) PAHs only. Larger PAHs ($>$50 C atoms) break somewhat with these trends (Bauschlicher, Peeters & Allamandola 2008), and the CH stretch is approximately twice as strong per CH mode for an ~100 C-atom cationic PAH than for a 50 C-atom cationic PAH. However, the interstellar 3.3-μm band can still safely be attributed to neutral PAHs given that what really counts for the observed spectra is the relative strength of the CH versus the CC modes, the number of CH modes per CC mode scales as $N_C^{1/2}$, and the fact that large PAHs do not get excited enough to contribute substantially to the CH stretching mode. Similar trends in intensity are evident for the CH out-of-plane deformation mode, but the same conclusion holds: The 11.2-μm mode results from neutral PAHs. This conclusion is supported by the much better agreement between the observed peak position of the 3.3-μm band and the calculated peak position of the CH stretching mode for neutral PAHs than for cations (Bauschlicher, Peeters & Allamandola 2008).

The spectra of PAH anions also show strong CC modes, but the strength of the CH modes relative to the CC modes is not as extremely low as for the cations. Anions are somewhat of a curiosity, though, in these spectral investigations. Presently, there are only high S/N spectra for sources with high surface brightness (e.g., PDRs). For PDR conditions, the fraction of anions is expected to be exceedingly small. PAH anions should be more abundant in the diffuse ISM (up to

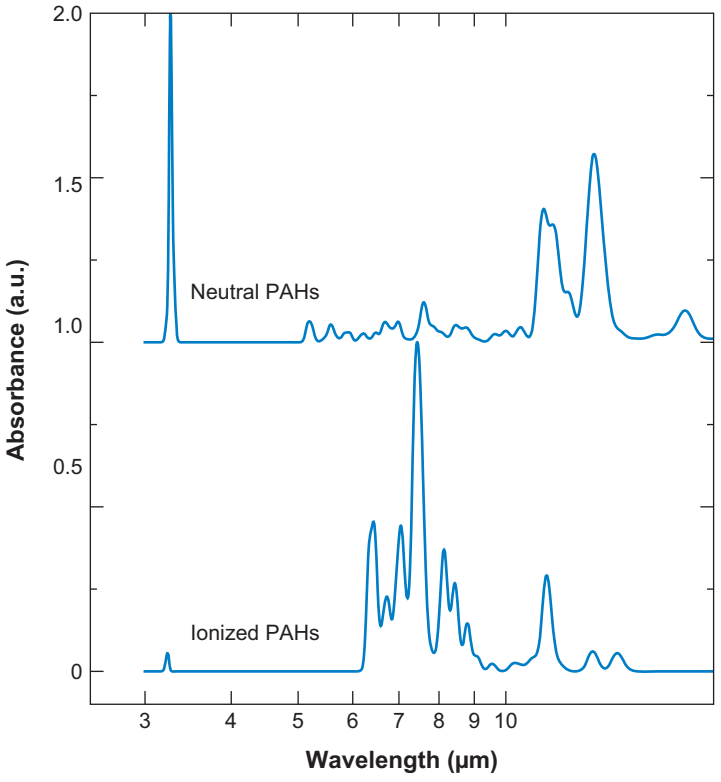

Figure 13

The absorption spectrum of a mixture of neutral polycyclic aromatic hydrocarbons (PAHs) (*top*) compared with the spectrum of the same species in their cationic states (*bottom*). The strength of the CC modes has increased considerably relative to the CH modes in the 3-μm and 11–15-μm region. Figure taken from Allamandola, Hudgins & Sandford 1999.

perhaps 20% of the PAHs, the rest in neutrals). Although this will give rise to appreciable intensity in the 6–9-μm CC mode region, it will hardly affect the CH mode characteristics.

Finally, the calculated spectra for large PAHs are largely limited to singly ionized PAHs. However, for larger PAHs, double ionization becomes particularly important in PDRs. Malloci, Joblin & Mulas (2007a) have calculated the spectral characteristics of a set of relatively small PAH dications (<70 C atoms). The specifics of the spectral characteristics of the dications have not been evaluated, but the results demonstrate that double ionization increases the intensity of the CC modes by another factor of 2 relative to the singly ionized PAHs. Bauschlicher & Bakes (2000) have also calculated the IR spectra of a few compact PAH dications. The results reveal little effect on the peak position of the 6.2-μm band.

In summary, all the laboratory and theoretical evidence points toward neutral PAHs as the carriers for the CH modes and cationic PAHs as the carriers for the CC modes in the interstellar spectra. This dichotomy is at the root of the observed variations in the ratio of the CH to CC modes (see Sections 2.2.1 and 3.6 and **Figures 3**, **6**, and **8**).

4.2.2. Size. Hudgins & Allamandola (1999a) have investigated the influence of PAH size on the IR characteristics for small PAHs using MIS. Large PAHs (up to 130 C atoms) can presently only be investigated using DFT (Bauschlicher & Bakes 2000; Bauschlicher 2002; Bauschlicher, Peeters

& Allamandola 2008). These studies reveal that the spectra of small PAHs (N_C < 50 C atoms) are diverse, and peak positions of the major bands shift around considerably. This possibly reflects the diversity of molecular structures represented in the small PAHs studied. In contrast, the calculated spectra of large PAHs (N_C > 50 C atoms) are much more uniform in appearance, but only highly symmetric, compact PAHs have been studied.

Perusal of these spectra reveals a shift in the peak position of the dominant CC mode around 6 μm from the 6.3-μm position (characteristic of class B) to shorter wavelengths with increasing size of the PAH cation. However, this trend is only present for PAHs with less than 30 C atoms and stops short of the ISM position of 6.2 μm (class A). There is no concomitant shift in the peak position of the major band near 7.7 μm for these small, cationic PAHs. For very large, compact PAHs, the peak position of the major bands becomes much more stable (Bauschlicher, Peeters & Allamandola 2008). In particular, the calculated CH stretch falls within a narrow range (∼0.003 μm) of 3.264 μm for large, neutral PAHs as compared with a range of ∼0.03 μm for all neutral PAHs. Similarly, the CH out-of-plane deformation mode region shows only two strong bands—the molecules studied contain only solo and duo H atoms—whose peak position falls within ∼0.05 μm of 11.0 μm and ∼0.15 μm of 12.6 μm. The large, compact, cationic PAHs studied have many allowed modes in the 6–9-μm range, but for some species, all the intensity is carried by a few modes, whereas for others, several bands show significant intensity. As a class, however, the spectra of large, compact, neutral and cationic PAHs are globally in line with the trends observed in the observed peak positions of the IR emission features—strong variations of the CC modes and only subtle changes in the CH modes (Bauschlicher, Peeters & Allamandola 2008). However, the observed peak position at 6.2 μm for ISM sources cannot be explained by large (or small), compact, ionized PAHs.

4.2.3. Substitution. The effect of substitution of various atoms in the carbon network has been studied systematically using DFT methods (Hudgins, Bauschlicher & Allamandola 2005; Bauschlicher, Peeters & Allamandola 2008). Of these, the class of polycyclic aromatic nitrogen heterocycles has been suggested to be particularly relevant to the analysis of interstellar spectra. Nitrogen is isoelectronic with CH and hence substitutes readily for a peripheral CH group in a neutral molecule. When nitrogen is substituted for carbon inside the carbon skeleton, the neutral species has a radical nature, whereas the cation becomes a closed-shell species. From the point of view of astronomical spectroscopy, the latter are the more relevant species. The calculations show that the peak position of the dominant IR active mode at approximately 6 μm shifts toward higher frequencies and that this shift is more pronounced when the N atom is located deeper in the ring structure (**Figure 14**). This spectral shift does not involve CN modes. Rather, the presence of nitrogen causes a redistribution of the electron density—nitrogen has a large electronegativity—which changes the dipole derivatives of the CC modes and hence the IR activity of the CC modes. The result is a shift toward higher frequency. As the molecule increases in size, this electron localization effect decreases in importance, and the shift is less pronounced. Substitution of multiple N atoms can counteract this dilution effect. If we assume that the typical size of the emitting PAH in space is 50 C atoms, then substitution with two N atoms is required to reproduce the observed peak position of the 6.2-μm band for class A sources (e.g., see Section 2.2.2) (Hudgins, Bauschlicher & Allamandola 2005).

The effects of other substitutions have also been investigated. Using silicon has little effect because its electronegativity is somewhat less than that of carbon. Oxygen has an even larger electronegativity than nitrogen. However, using oxygen destroys the aromaticity of the species; hence it substitutes only readily as a peripheral group. The resulting shift is then too small to be responsible for the observed blue position of the interstellar 6.2-μm band (Hudgins, Bauschlicher & Allamandola 2005).

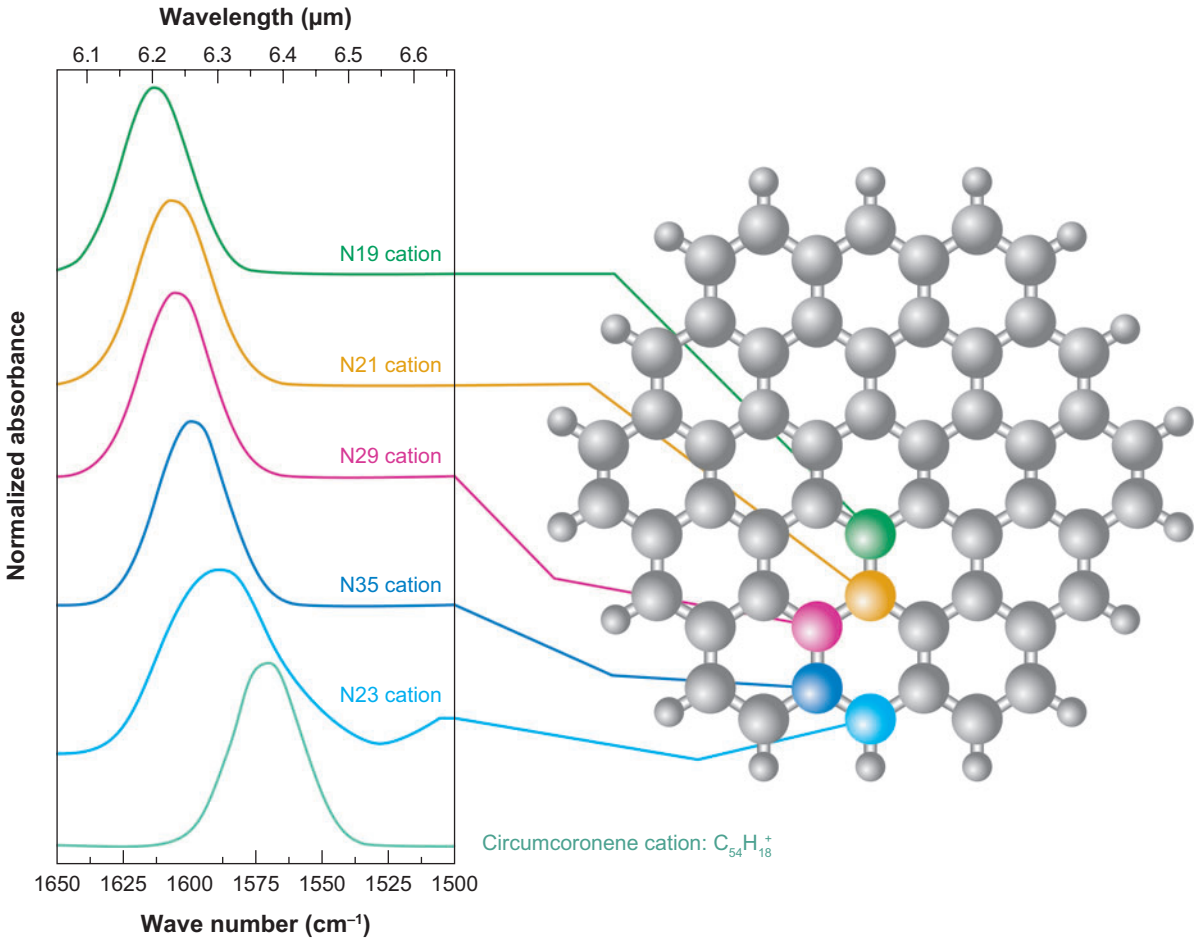

Figure 14

Density functional theory calculated spectra of the circumcoronene cation with one N atom substituted for one C atom calculated in the 6-μm region (Hudgins, Bauschlicher & Allamandola 2005). The location of the N atom in the carbon skeleton is indicated on the right. The corresponding spectrum is shown on the left. Note that the peak position shifts to higher frequencies when the N atom is substituted deeper in the species.

Rather than substitution, metal atoms form complexes with PAHs in which they are situated above or below the plane. Such complexes have been investigated with DFT calculations, and a few iron complexes with small PAHs have been measured using the MPD technique (Hudgins, Bauschlicher & Allamandola 2005; Szczepanski et al. 2006; Simon & Joblin 2007). The calculations suggest that, for the iron-coronene complex, the charge resides on iron, and the calculated peak position of the 6.2-μm band may shift all the way to 6.1 μm (Hudgins, Bauschlicher & Allamandola 2005; Simon & Joblin 2007).

4.2.4. Clusters. The large polarizability of PAH molecules provides a strong bonding force between the aromatic planes of PAHs. Typically, the van der Waals interaction energy between neutral PAHs is approximately 0.05 eV per C atom (Zacharia 2004). Such clusters represent an important link between molecular and solid-state branches of soot formed in flames (**Figure 15**). Where this

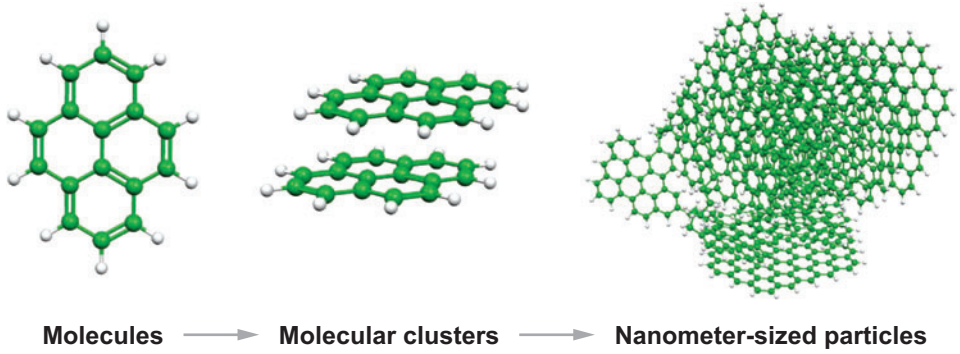

Figure 15

Polycyclic aromatic hydrocarbon (PAH) clusters form the bridge between individual PAH molecules and amorphous carbon nanoparticles.

transition from two-dimensional planar structures to three-dimensional nanograins occurs is not well known. Studies on PAH clusters have focused on the stability and structure of fairly small clusters (Klotz et al. 1995; Bréchignac et al. 2005; Rapacioli et al. 2005, 2006). A PAH cation or anion bonds strongly to neutral PAH molecules by charge-induced dipole bonding, which is expected to be an even stronger bonding mechanism. Because the charge-induced bonding mechanism has a much longer range than van der Waals bonding, PAH ionization should enhance cluster formation.

There has been much interest in the IR characteristics of clusters. Specifically, one component identified in principal component analysis of spectral maps of the IR emission features has tentatively been identified with clusters (Rapacioli, Joblin & Boissel 2005). PAH clusters may also be the carriers of the plateaus underlying many emission features (Bregman et al. 1989) and they may be related to the very small grains, thought to be responsible for the 25-μm cirrus discovered by the Infrared Astronomical Satellite mission. In addition, in terms of material properties, clusters form a link between the molecular properties of PAHs and the bulk-derived properties of classical grains. Because of the lack of a suitable numerical method, the intrinsic properties of PAH clusters and the differences with planar PAHs are largely unexplored.

4.3. Specific Identification

Although the presence of large PAH molecules in space is undisputed, identifying specific species has remained challenging. That is not surprising because the mid-IR spectral range is characteristic of fundamental vibrations involving nearest-neighbor atoms, which are not sensitive to the larger molecular structure. The 15–20-μm spectral range probes (next-nearest neighbor) deformation modes of the carbon skeleton (see Section 3.8), but these have only limited diagnostic value when similar molecular structures are present in the PAH family. The lowest-lying vibrational modes offer the best hope to identify PAHs through their vibrational transitions. Similarly, the electronic spectrum of PAHs is characteristic and can be used for fingerprint purposes. Traditionally, the pure rotational spectrum of molecules has been used to identify molecules in space. All these avenues have been explored in recent years in a quest to identify the specific PAHs present in space.

4.3.1. Diffuse interstellar bands and electronic transitions. The DIBs compose a set of visible absorption bands discovered almost 100 years ago in stellar spectra. The DIB spectrum is rich, with some 200 DIBs known. DIBs show a wide range in strength (from $\Delta\tau/Av \sim 0.1$ to the grass limit)

and width (0.5–50 Å). The (stronger) DIBs correlate reasonably but not perfectly with each other. Generally, these absorptions are now attributed to electronic transitions in an extended family of molecular species. Depending on the oscillator strength of the transitions involved, ~0.1% of the elemental carbon is locked up in the carrier ($f = 1$). Overviews of the field can be found in Tielens & Snow (1995) and Herbig (1995). Despite vigorous efforts by the world's leading spectroscopy groups, the identification of these bands with specific carriers has remained enigmatic.

Interstellar PAHs have often been suggested as possible carriers of the DIBs. Arguments in favor of this possibility include their known presence in space, the high abundance of these species in the ISM, and their photochemical stability under interstellar conditions. Because small neutral PAHs do not absorb in the visible region of the spectrum, the focus has been on ionized PAHs as DIB carriers. Several laboratory groups have studied the visible spectra of PAH cations using various experimental techniques, such as MIS, van der Waals clusters, and cavity ring-down spectroscopy (Bréchignac & Pino 1999, Salama et al. 1999, Ruiterkamp et al. 2002). Despite tantalizing claims, no unambiguous identification has been made with a specific PAH species. The key problem seems to be that the focus has been on relatively small species whose first electronic transition occurs in the visible but is weak, and, at the grass level, any species produces a hit. The $S_2 \leftarrow S_0$ or $D_2 \leftarrow D_0$ transitions in these species are much stronger. However, in that case, internal conversion is rapid, and these transitions are too broad to be relevant for the DIBs (or, to phrase it differently, such broad absorptions would have been missed in current interstellar surveys) (T. Pino & P. Brechignac, private communication). From this perspective, it seems unlikely that the DIBs are carried by interstellar PAH molecules.

Alternative identifications, following the original suggestion by Douglas (1977), include a variety of carbon chains. Here too tantalizing claims have not held up against detailed scrutiny. Carbon chains face similar challenges as the PAHs. Open-shell species (even-number C atoms) have weak first transitions. Their second transitions have reasonable strength, but only relatively large species (e.g., C_{20}) absorb in the visible (Maier, Walker & Bohlender 2004; Maier et al. 2006). Rapid internal conversion rates and hence broad absorption bands are issues as well (Maier et al. 2006). The odd-numbered chains, conversely, do have relatively strong first transitions, and for the species C_{15} to C_{31}, these occur in the 4000–9000-Å region of the spectrum. Given the required photostability, only species with sizes in the upper range are expected to have appreciable abundances in the ISM. Following the discussion in Section 5.4.3, these chains and rings may result from isomerization reactions of fully dehydrogenated PAHs. Further gas-phase reactions with H, C^+, and C, as well as UV dissociation, may then lead to a select number of abundant species.

Finally, molecular electronic transitions in the FUV are typically strong. However, the rapid internal conversion rates for second or higher electronic transitions are likely a general characteristic of molecular absorptions; hence, DIBs in the FUV are likely to be much broader than visible DIBs and therefore difficult to detect. The observational data on DIBs show a general trend for an increase in width with increasing frequency (Herbig 1975).

4.3.2. Low-lying ro-vibrational transitions. The lowest vibrational modes of PAHs involve deformation modes of the carbon skeleton and hence are characteristic of the molecule involved. Moreover, emission in these modes occurs late, after the absorption of the FUV photon, when most of the energy has decayed away through emission in the mid-IR modes. At low internal energies (approximately 1000 cm^{-1}), the vibrational modes of a species decouple, and rather than broad bands, the emission is characterized by the typical ro-vibrational PQR structure (**Figure 16**) (Mulas et al. 2006b). The separation of the individual bands reflects the rotational constants and thus the moments of inertia of the molecule. The location of the Q branch, coupled with the

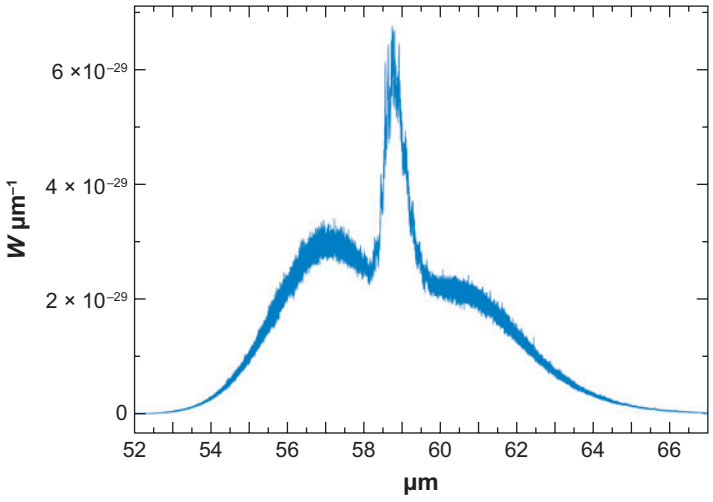

Figure 16

The lowest vibrational modes of polycyclic aromatic hydrocarbon molecules show characteristic PQR branches. The detailed rotational structure depends on the difference in rotational constants between the ground and excited vibrational states. This calculation is appropriate for naphthalene, for which the rotational constants have been theoretically evaluated (Mulas et al. 2006b). An intrinsic line width of 1 km s^{-1} has been adopted in this calculation.

separation of the individual P and R transitions, thus provides a powerful tool for the identification of the specific PAH species present in space (Mulas et al. 2006b).

There is little experimental data on the far-IR vibrational modes of PAHs. The thermal emission of five small PAHs has been measured in a gas-phase cell using a Fourier transform spectrometer (Pirali et al. 2006). DFT calculations have also been reported (Bauschlicher 2002; Pirali et al. 2006; Malloci, Joblin & Mulas 2007b). These studies reveal the importance of out-of-plane motions and butterfly modes for PAHs with peripheral hexagons, but in general the motions involved in the modes are complex. For the series of compact PAHs (coronene, circumcoronene, and circumcircumcoronene), the lowest vibrational modes show a regular shift toward lower frequencies from 113.9, to 54.5, and 30.1 cm^{-1}. Joblin and coworkers (Mulas et al. 2006a,b) have modeled the expected far-IR emission of interstellar PAHs. The results show that the fraction of the energy emitted in the lowest modes of coronene is, not surprisingly, small, ∼0.2% of which one-third is emitted after decoupling. If we assume that the PAHs carry 10% of the total IR emission and that there are 50 equally dominant, interstellar PAHs, the intensity of the Q branches for a single species is $\sim 10^{-6}$ of the total IR emission. Hence, line-to-continuum is a concern and the observations are daunting. Nevertheless, observing a bright PDR (in which the peak of the dust continuum falls at relatively short wavelengths) at high spectral resolution seems feasible. The lowest vibrational modes of compact PAHs shift through the Herschel and SOFIA range when they shift through the astrophysically relevant size range of 20 to 100 C atoms. Similar considerations also apply to other molecular species, in particular the lowest vibrational modes of carbon chains. Herschel and SOFIA could thus provide important handle on the molecular complexity of the universe.

4.3.3. Rotational spectroscopy. Neutral PAHs generally do not possess a permanent dipole moment and hence have no allowed pure rotational spectrum. Exceptions include nonplanar species such as the bowl-shaped corannulene and other species with five-membered rings, as well as open-shell species such as PAHs with substituted nitrogens. Cations also have dipole moments

and should give rise to a rotational spectrum. Only a few very small species have been investigated in the laboratory (see Thorwirth et al. 2007, and references therein). Although this data will facilitate radio-astronomical searches, the large partition function for these species will hamper detection.

The presence of a component of anomalous microwave (10–100 GHz) excess emission was first realized based on a comparison of results from the Cosmic Background Explorer Differential Microwave Radiometer with the DIRBE dust emission at 140 μm and has now been shown to be characteristic of the galactic emission spectrum (Kogut et al. 1996). This galactic foreground (as known to cosmologists) emission has been attributed to emission from spinning interstellar dust grains (Draine & Lazarian 1998). Models show reasonable agreement with the observations (Draine & Lazarian 1998). It is within this emission that the PAH rotational emission has to be searched. The rotational population of PAHs is set by a balance of vibrational photon emission with the rotational photon emission (Rouan et al. 1992), and moderately large PAHs ($N_C \simeq 300$) can reach high rotational temperatures ($T_{rot} > 500$ K). The individual transitions may then disappear in the grass, limiting the use of these transitions for identification purposes. There have been no quantitative studies to address these issues.

5. POLYCYCLIC AROMATIC HYDROCARBONS AND THE CHEMISTRY OF THE INTERSTELLAR MEDIUM

A variety of processes play a role in the chemistry of PAHs in the ISM. First and foremost, the interaction of PAHs with UV photons is a key factor in controlling the composition of the interstellar PAH family. Similarly, reactions with abundant atoms—H, C, C^+, N, and O—are of interest. Finally, inside dense clouds, PAHs may be accreted into ices and then photolyzed by (cosmic-ray-created) FUV photons. The products may then be released into the gas phase through thermal heating in the hot cores and corinos associated with star-forming and planet-forming regions or in PDRs associated with HII regions. Sputtering by cosmic rays or in C-shocks may also return the products to the gas phase.

5.1. Photochemistry

At low energies, photoionization is the only channel open. Photoionization yields have been measured by Verstraete et al. (1990) and by Jochims, Baumgärtel & Leach (1996). For the few small PAHs measured, the results show a rapidly increasing yield, Y_{ion}, above the ionization potential, IP, which is well described by a simple rule: $Y_{ion} \simeq (h\nu - IP)/9.2$ for photon energies, $h\nu$ less than $IP + 9.2$ eV, and unity above this energy (Jochims, Baumgärtel & Leach 1996).

At higher energies, PAH photodestruction channels open up. The photostability of PAHs has been studied experimentally by Jochims et al. (1994; Jochims, Baumgärtel & Leach 1999) and Gotkis et al. (1993). These studies provide direct information on the disappearance energy—defined as the internal energy at which the dissociation rate is approximately 10^4 s^{-1}—as well as the loss channel involved (hydrogen loss versus fragmentation) for a few small PAHs (up to 24 C atoms) and the effect of methyl side groups, as well as additional peripheral H atoms (e.g., hydro-PAHs). The photo(in)stability of PAHs is of course also put to good use in the MPD spectroscopic technique (see Section 4.1.2). The photodissociation of PAHs has also been studied using DFT to determine bond-dissociation energies in relevant loss channels (Jolibois et al. 2005).

A number of theoretical studies have assessed the importance of fragmentation of highly vibrationally excited PAHs in space (Geballe et al. 1989; Allain, Leach & Sedlmayr 1996; Le Page, Snow & Bierbaum 2001, 2003; Tielens 2005). These studies are based on unimolecular

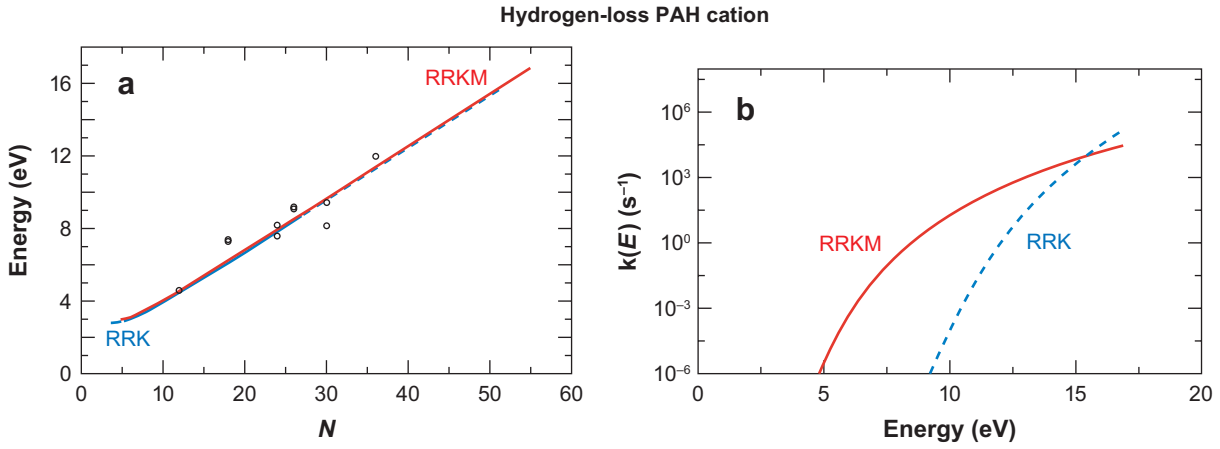

Figure 17

(*a*) The measured internal energy at which hydrogen loss occurs as a function of the number of C atoms in the species. Experimental data (*open circles*) taken from Jochims, Baumgärtel & Leach (1994). The lines are fits to these data based on unimolecular theory (RRKM, *solid red line*; RRK, *dashed blue line*) with the dissociation energy as a free parameter. (*b*) The unimolecular dissociation rate for hydrogen loss from a 50 C-atom polycyclic aromatic hydrocarbon (PAH) cation as a function of internal energy calculated with the RRK and RRKM model using the dissociation energy fitted in panel a. Both models are fitted to the experimentally measured dissociation rate at an internal energy of 15 eV but extrapolate to different dissociation rates for lower energies. Figure taken from Tielens 2005.

dissociation theories of increasing sophistication, used to extrapolate from the small measured PAHs to the much larger PAHs relevant in space. Moreover, the dissociation rates measured in the laboratory have to be compared to IR radiative stabilization rates (approximately 1 s^{-1}) to arrive at the dissociation probability upon photon absorption. Because the long timescales in space allow a photoprocess to occur repeatedly, a photoprocess can still be relevant even with a low intrinsic probability. In addition, multiphoton processes—in which a PAH absorbs a second photon before it has radiated the energy of the first photon away—have a low probability but can be important as well, particularly in regions near bright UV sources (e.g., protoplanetary disks, active galactic nucleus). The pitfalls associated with this have been discussed (Tielens 2005).

When evaluating these studies, it should be realized that calculated bond energies are not quantitative values to be used in these extrapolations. Generally, the energy required in a bond for dissociation and/or the number of effective oscillators over which the internal energy can be distributed is left as a free parameter in fits to measured rates. **Figure 17** illustrates the salient points. The existing experimental data are equally well fitted at different levels of theory, but this results in different bond-dissociation energies. Although RRK and RRKM both fit the measured experimental rate (10^4 s^{-1}), they provide different estimates for the internal energy required for hydrogen loss under astrophysically relevant conditions. Specifically, using RRK theory, the internal energy required for hydrogen loss (at $k = 1$ s^{-1}) is ~12 eV, whereas the RRKM theory—which describes the density of states much more accurately—requires only ~8 eV (**Figure 17**). Although this discussion focuses on hydrogen loss, the uncertainty in the fragmentation rates of the carbon skeleton is even larger because only limited experimental data exist on this process to guide the estimates. Nevertheless, calculated bond energies provide good insight into the relative importance of a loss channel; e.g., carbon loss (i.e., C_2H_2 loss) is much slower than aromatic hydrogen loss, whereas hydrogen loss from a methyl group or hydrogroup is faster than aromatic hydrogen loss (Jochims et al. 1994; Jochims, Baumgärtel & Leach 1999).

5.2. Gas-Phase Chemistry

Bohme (1992) presented an early review of gas-phase chemistry involving PAHs, including a discussion of the thermochemical properties of PAHs and related species. At that time, reactions were mainly limited to those involving benzene and naphthalene (and the fullerenes C_{60} and C_{70}). In subsequent years, a number of groups have started to expand this to larger PAHs.

Electron attachment to PAHs ($PAH + e \rightarrow PAH^-$) has been studied in the laboratory by two groups (Tobita et al. 1992, Abouelaziz et al. 1993, Canosa et al. 1994) and theoretically estimated by Allamandola, Tielens & Barker (1989). The electron-attachment cross section depends strongly on the electron affinity of the neutral PAH and small PAHs (<25 C atoms), with electron affinities below 1 eV having low attachment rates because the intermediary, excited, anion complex autoionizes readily before photon emission can stabilize the anion (Tielens 2005). The electron-attachment rate measured for anthracene is only approximately 10^{-9} cm^3 s^{-1} (Canosa et al. 1994), which corresponds to an electron sticking coefficient of 10^{-4}. This is consistent with an electron affinity of 0.85 eV, within the measured range of 0.4–1 eV (Tobita et al. 1992). Larger PAHs have higher electron affinities and hence can have electron sticking coefficients close to unity. A high electron-attachment rate, however, is contingent on the existence of accessible low-energy negative ion states in which capture can occur (*s*-wave capture). Some species—notably the fullerenes C_{60} and C_{70}—can efficiently attach electrons at elevated temperatures ($T > 2000$ K) through the *p*-wave capture process; however, a small energy barrier inhibits the formation of anion *s* states and results in a low electron-attachment rate at low temperatures (Smith, Spanel & Mark 1993). Not all PAHs show low-lying anion resonances in their electron-scattering cross section; hence these few experimental results cannot be confidently extrapolated to all (large) PAHs. Indeed, some PAHs in the astronomical family may efficiently form anions, whereas others do not.

Charge-exchange reactions involving neutral PAHs ($PAH + M^+ \rightarrow PAH^+ + M$) have only been measured for anthracene with C^+, Ar^+, and He^+ (Canosa et al. 1995). These reactions proceed at the Langevin rate (2–6 $\times$ 10^{-9} cm^3 s^{-1}, depending on the species involved). For most species, the exothermicity of the reaction is a few electron volts, and charge exchange is the only channel open at low temperatures. The reaction with C^+ can also lead to carbon insertion, and a branching ratio of 0.6:0.4 has been estimated for charge transfer versus insertion for anthracene (Canosa et al. 1995). Insertion probably proceeds through addition in the π-system followed by the formation of a cyclopropa-PAH peripheral group. He^+ provides another possible exception because the excess energy leaves the cation highly excited and may even lead to double ionization. The doubly ionized PAH may then fragment either through direct processes or through Coulomb explosion (Leach 1987). Experiments provide some support for the occurrence of both these processes for anthracene ($\Delta IP \simeq 17$ eV for singly ionized anthracene).

Electron recombination rates ($PAH^+ + e \rightarrow PAH$) have been measured for a few small PAH cations using a modified flowing afterglow Langmuir probe technique in which ions and electrons are carried by an inert gas, and the ion and electron population are followed at several points downstream using a moveable mass spectrometer and Langmuir probe, respectively. A steady-state concentration of PAH cations is produced through charge exchange with inert gas (helium/argon) ions created in an afterglow (Biennier et al. 2006). Photoionization by a carefully tuned laser increases the local PAH cation concentration, whose time evolution can then be followed by the mass spectrometer. Electron recombination rates have been measured at room temperature for the small PAH cations naphthalene, azulene, acenaphthene, anthracene, phenanthrene, fluoranthene, and pyrene (**Figure 18**). These rates have to be extrapolated to larger, astrophysically more relevant PAHs. Some theoretical studies directly adopt these rates in astronomical models for all sizes of PAHs, albeit sometimes scaled with $T^{-1/2}$ to the low temperatures of the ISM. Other studies

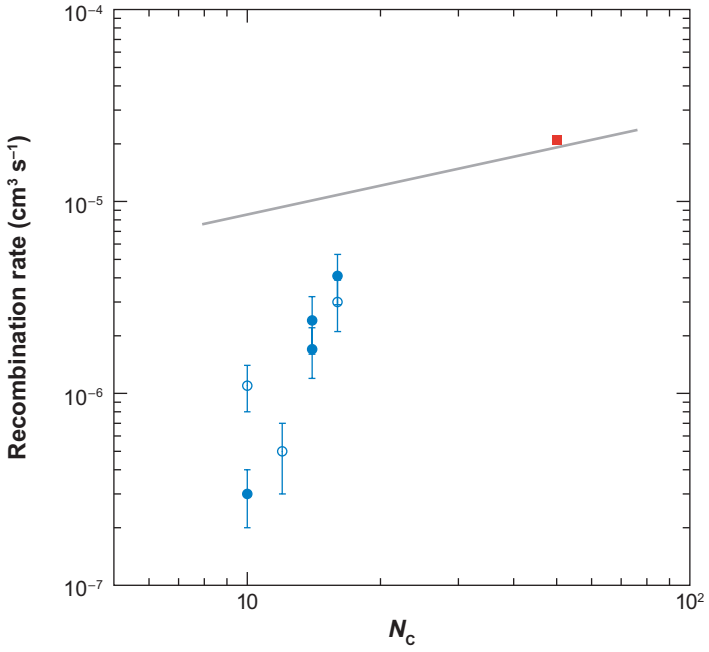

Figure 18

Experimentally measured electron recombination rates of polycyclic aromatic hydrocarbon cations: those with only six-membered rings (*blue filled circles*) and those with one five-membered ring (*blue open circles*). The red square indicates the value derived from the ion fraction implied by the observed CC/CH modes in the Orion Bar. The line shows the theoretical electron recombination rate for a thin conducting disk. Figure adapted from Biennier et al. 2006.

assume an $N_c^{1/2}$ dependence for the recombination rate. Finally, some models depend exclusively on theoretical rates appropriate for a thin conducting charged circular disk, which account for the Coulomb interaction as well as the image charge and assume a unit electron sticking coefficient (see Tielens 2005). The theoretical rate is somewhat larger than the experimentally measured rates for small PAHs, which may reflect that a conducting circular disk is not a good approximation for the structure and characteristics of the measured small PAH cations (**Figure 18**).

There are no experimental measurements for the mutual neutralization reaction of PAH anions with atomic or molecular cations ($PAH^- + M^+ \rightarrow PAH + M$). Yet these reactions are key to the ionization balance in atomic and molecular clouds. Theoretical estimates are based on the interaction of ions with small, negatively charged grains. However, extrapolating the classical formula from grains to small PAHs may be problematic for electron recombination rates and may also break down for charge-exchange reactions involving atomic ions and neutral PAHs.

Reactions involving PAH cations; H, N, and O atoms; and the H_2 molecule have been measured by the Boulder group (Snow et al. 1998; Le Page et al. 1999a,b; Betts et al. 2006). The results show that PAH cations react readily with H and O atoms ($1.5–2 \times 10^{-10}$ and approximately 10^{-10} cm^3 s^{-1}, respectively), forming (for large PAHs) exclusively an association product. Reactions with nitrogen do occur at a similar rate for very small PAHs, leading mainly to HCN formation. However, the reaction rate constant decreases rapidly with PAH size, and no reaction is observed for coronene. No reactions are observed with H_2. However, dehydrogenated benzene and naphthalene (but not pyrene) abstract an H atom from H_2. Similarly, no reaction is observed for the pyrene cation with the molecular species CO, H_2O, and NH_3. The Rennes

group (Goulay et al. 2005, 2006) has studied the reactivity of (neutral) anthracene with CH and OH radicals. These reactions occur at the collision rate with no sign of an activation barrier down to gas temperatures of 60 K, and adducts are likely formed.

5.3. The Chemistry of Polycyclic Aromatic Hydrocarbons in Ices

The chemistry of PAHs in ices has been studied by Bernstein and coworkers (Bernstein, Sandford & Allamandola 1996; Bernstein et al. 2002). Energetic processing by UV irradiation or ions of ices with trapped PAHs leads to efficient replacement of aromatic hydrogen by functional groups such as OH, CH_3, COOH, CN, and CO (depending on the ice mixture) at doses appropriate for molecular clouds. The carbon skeleton, however, is not affected. Although this energetic processing may have relevance for the organic inventory of Solar System bodies such as meteorites, asteroids, satellites, and comets, it is likely not a driving force for the incorporation of nitrogen inside the carbon skeleton posited as an explanation for some observed spectral variations (see Section 3.7). The photostability of benzene and nitrogen-substituted benzene in ices has been investigated by the Ehrenfreund group (Peeters et al. 2005, Ruiterkamp et al. 2005). The results show that these (small) species can survive inside dense clouds but not in the diffuse ISM, as expected (see Section 5.4.3). Overall, the importance of PAH processing in ices in molecular clouds has not been quantitatively assessed.

5.4. Origin and Evolution of Interstellar Polycyclic Aromatic Hydrocarbons

Here, we review the different processes that may affect the evolution of PAHs in space, including soot chemistry in stellar ejecta, shattering of carbonaceous grains in interstellar shocks, and gas-PAH reactions in the ISM.

5.4.1. Origin of polycyclic aromatic hydrocarbons in asymptotic giant branch stars. From a chemical viewpoint, PAHs are characteristic of high-temperature products in sooting environments, and in an astrophysical setting, carbon-rich AGB stars provide a likely origin for interstellar PAHs (Latter 1991). Observationally, however, there is little direct support for PAHs in outflows from carbon-rich AGB stars. This likely results from the absence of UV pumping photons in the stellar spectra as stars cooler than 4000 K generally show no evidence for the IR emission features (see **Figure 20**). Following an early study by Buss, Tielens & Snow (1991) based on Infrared Astronomical Satellite/Low-Resolution Spectrometer spectra, the IR emission features have been detected in ground-based and ISO/SWS spectra of the carbon-rich AGB star TU Tau (Boersma, Hony & Tielens 2006; Speck & Barlow 1997). In this case, the emission features are likely pumped by the blue binary companion. Recently, Sloan et al. (2007) detected the IR emission features in the carbon-rich star HD 100764. This warm (4800 K) R-type carbon giant is surrounded by a thin disk, which is the likely location of the emitting PAHs. The enigmatic, early R carbon stars probably form through mergers in binary systems, and the disk likely represents captured carbon-rich ejecta before or during this process.

Although carbon-rich AGB stars generally do not show the IR emission features, carbon-rich post-AGB objects and PNe invariably do. The presence of PAHs in the spectra of these AGB-star descendants may merely reflect the increased effective temperature of the central object as it loses its remnant envelope and shifts to the blue in the Hertzspring-Russell diagram, on its way to becoming a white dwarf. In any case, the presence of PAH features in the IR spectra of carbon-rich post-AGB objects and PNe lends indirect support for the importance of late-type stars as sources for PAHs in the ISM.

In analogy to soot formation in terrestrial environments, dust formation in the outflows from carbon-rich AGB stars is thought to proceed through the nucleation of small PAH species. Theoretical studies on PAH formation in AGB envelopes have been performed by Frenklach & Feigelson (1989) and Cherchneff, Barker & Tielens (1992). The processes that convert C_2H_2 into large PAH molecules and eventually soot are similar to those occurring in the pyrolysis of hydrocarbon molecules. There is an extensive literature on PAH and soot formation in combustion environments, largely driven by internal combustion engine efficiency, pollution, and health-hazard concerns. Several different chemical pathways toward soot have been proposed based on neutral radicals, ions, polyacetylene chains, or fullerenes, and each may dominate in different environments as different factors drive the system to the thermodynamically most favored state. Their high stability, the high tendency of aromatic fuels to soot, and the structural similarity between the carbon backbone of PAHs and soot have led to the notion that PAHs are building blocks—the condensation nuclei—of soot particles. Indeed, carbon-sooting flames typically produce ~5% of the available carbon in small PAHs.

Detailed reaction networks have been proposed for the chemical reaction routes that lead to PAHs in AGB outflows. These are based on terrestrial sooting studies and generally employ measured reaction rates for the first steps in this process—closure of the first ring and growth of the second ring—and reasonable estimates for the rates of similar reactions during the subsequent growth stages. These are then incorporated in models for AGB winds at various levels of approximation. For typical stationary outflow parameters, the results show that PAH formation is inefficient (10^{-5}) (Cherchneff, Barker & Tielens 1992). However, this conclusion may reflect our limited understanding of the actual physics involved in these outflows rather than an inherent problem in forming PAHs in such environments. After all, these objects form copious amounts of soot, and these grains have to pass through a PAH-like condensation nuclei state. Hence, recent studies have addressed this issue, for example, by exploring the effects of shocks driven by the photospheric pulsations, which lift the photosphere to large distances from the stellar surfaces at which the gas is cool and dense, promoting the chemical growth of PAHs (Cau 2002). This results in higher PAH yields (3×10^{-3}), although still somewhat less than needed to explain the observed high fraction of elemental carbon in PAHs in carbon-rich post-AGB objects and PNe and in the general ISM.

The presence of di- and triacetylene chains, as well as the possible identification of benzene in the IR spectrum of AFGL 618 (Cernicharo et al. 2001), has led to the suggestion that the combination of high densities, high temperatures, and high ionization rates drives an efficient ion-molecule chemistry involving condensation reactions of acetylene in these post-AGB environments (Woods et al. 2002). Alternatively, these species are formed in the PDR zones by a rich photochemistry (Cernicharo 2004). This rich chemistry may lead to larger PAH species as well.

5.4.2. Polycyclic aromatic hydrocarbons and interstellar shocks. Interstellar shocks may be an important source of PAHs through the fragmentation of graphitic grains. Supernova explosions drive strong shock waves into the ISM, which convert the kinetic motion of the gas into thermal energy. However, because of their inertia, the grains plow through the warm gas. Moreover, the grains are charged and therefore gyrate around the magnetic field. Upon compression of the postshock gas, grains can then be betatron accelerated, and high velocities can be maintained over a large column density of gas. Collisions between large and small grains can then lead to cratering or even catastrophic destruction of the whole grain. The critical pressure for crater formation is approximately 4×10^{10} dyn cm^{-2}, corresponding to critical impact velocities of approximately 1 km s^{-1} (Jones, Tielens & Hollenbach 1996). This translates into the catastrophic destruction of a 1000-Å grain by a 50-Å grain at a critical velocity of approximately 75 km s^{-1}. Although the critical velocity for crater formation by micrometer-sized impacts has been determined experimentally,

the larger velocities needed to catastrophically destroy large grains is beyond present experimental techniques. Laser acceleration techniques—using the National Ignition Facility—may provide an opportunity to study this process in the laboratory. Also, there is presently little experimental data on the size distribution resulting from submicrometer grain-grain collisions. Theoretical studies result in $n(a)da \sim a^{-3.3}da$, but the minimum size is not constrained (Jones, Tielens & Hollenbach 1996). Given the layered structure of graphitic materials, however, the smallest fragments likely are small, two-dimensional structures (e.g., PAH-like molecular species). Further processing by reactive atomic H, C^+, and C, as well as UV photoprocessing, may then quickly further transform these species into compact PAHs in the ISM.

Jones, Tielens & Hollenbach (1996) have evaluated this model for the origin of PAHs in shock waves. The results show that shattering caused by grain-grain collisions is an important process for the evolution of the interstellar grain-size distribution. The calculated lifetime of a large (approximately 1000 Å) grain—against shattering—is actually uncomfortably short, 10^8 years. A typical interstellar shock, $v_s \sim 100$ km s^{-1}, may transform ~10% of the solid carbon into small carbon clusters (<15 Å); hence this may be a viable mechanism for the production of interstellar PAHs, PAH clusters, and very small grains (Jones, Tielens & Hollenbach 1996). These shock models do not account for the destruction of PAHs by sputtering in the postshock gas. Although this is likely not relevant for 100 km s^{-1} shocks in which PAHs are quickly stopped in the gas, processing by faster shocks may be relevant for the evolution of the interstellar PAH population.

There is presently little evidence for the presence of PAHs in regions processed by supernova shocks. Largely, this reflects the difficulty of discerning the emission of supernova remnants (SNRs) against that of galactic background material. Thus, although gas heating is rapid and cooling is inefficient (resulting in high temperatures and a characteristic UV and visible emission line spectrum), PAHs and dust grains are heated slowly, cool efficiently, and generate little excess emission (above that generated through the absorption of UV radiation). Reach et al. (2006) have identified four SNRs out of a sample of 95 whose IR colors suggest excess emission from PAHs, but most sources were too confused by the background. The Large Magellanic Cloud may provide the best opportunity to address the presence of PAHs in shocked gas, given its nearness and almost face-on appearance, limiting background confusion. A study of the SNR N132D in the Large Magellanic Cloud revealed the presence of a steeply rising mid-IR continuum and weak emission features at 16.4 and 17.4 μm (Tappe, Rho & Reach 2006). These features are attributed to relatively large carbon PAH species ($N_C \sim 4000$ C atoms), which may be able to survive ~100 years in the hot (8×10^6 K) gas associated with the strong shocks in this young (~2500 years) SNR. Finally, PAH emission has been detected associated with the superwind driven by the nuclear starburst in M82, some 8 kpc above the plane (Engelbracht et al. 2006). These species have been entrained by the hot shocked gas and transported upward into the halo, in which they have survived ~10^6 years under extreme conditions.

5.4.3. Chemical evolution of polycyclic aromatic hydrocarbons in the interstellar medium.

Astronomical models are lagging in the area of the chemical evolution of PAHs in the ISM. Le Page, Snow & Bierbaum (2003) performed the most complete study of the effects of hydrogenation and dehydrogenation of interstellar PAHs. Existing studies agree that the dissociation rate decreases rapidly with increasing PAH size; hence the size at which PAHs transition from being strongly affected by photoprocessing to not being affected at all is sharp. Thus, small PAHs rapidly lose all hydrogen atoms when the rehydrogenation rate cannot keep up with the photochemical loss of aromatic hydrogen. Estimates of the critical size for which this becomes important range from approximately 25 to 50 C atoms (Le Page, Snow & Bierbaum 2003; Tielens 2005), and 35 C atoms is a reasonable value. This critical size scales with G_o/n_H. Thus, in moving from diffuse interstellar

clouds ($G_o/n_H \simeq 0.02$) to PDRs ($G_o/n_H \simeq 1$), this critical size decreases, but this size difference is only approximately five C atoms. The formation of hydro-PAHs (PAHs with extra H atoms) is generally unimportant in HI regions because of the low binding energy of such adducts (Le Page, Snow & Bierbaum 2003).

In principle, very small PAHs can rapidly lose C_2H_2 through UV photon absorption. However, this direct carbon loss is likely not the dominant photochemical destruction channel for the carbon skeleton because the critical size involved is much less than for hydrogen loss. Rather, hydrogen loss results in completely dehydrogenated PAHs, which may isomerize to carbon chains or rings, removing small species from the PAH family (Joblin 2003). The resulting carbon chains and rings are similarly susceptible to carbon loss upon photon absorption, which should be balanced by insertion reactions with gas-phase carbon (PAH cations) or C^+ (neutral PAHs) (Le Page, Snow & Bierbaum 2003). In their studies of molecular abundances in the Horsehead nebula, Teyssier et al. (2004) and Pety et al. (2005) suggested that this balance may be the origin of small, gas-phase carbon species (particularly, C_2H, c-C_3H_2, C_4H) in the PDR. Although this is an appealing picture for the role of PAHs in the synthesis of carbon species in the ISM, and schematic models look promising (Thaddeus 1995, Bettens & Herbst 1997), little has been done in terms of quantifying this model in terms of either specifying chemical routes toward specific species backed up with measured reaction rates and products (simulating well-studied sources) or evaluating quantitively the contribution of PAHs over their lifetimes in the ISM. Therefore, it is presently unclear how important these routes are in comparison with more traditional astrochemistry in which carbon-bearing species are built up through C^+ or C insertion reactions, acetylene condensation reactions, and/or neutral-neutral reactions. As noted by Thaddeus (1995), there is an important issue here: The rapid reaction of the abundant species, C^+/C, with (large) PAH, PAH cations, or very small grains should lead to a rapid depletion of gas-phase carbon in the diffuse ISM. Possibly, the carbon added by this reaction is susceptible to subsequent removal through its reaction with atomic or molecular hydrogen, returning the carbon to the gas phase as a small radical. Based on depletion data (and unlike silicon, magnesium, iron, and many other elements), carbon does not seem to partake in grain surface chemistry in the diffuse ISM. This lack of depletion variations of carbon in the diffuse ISM is not understood and presents a general problem for interstellar depletion models.

The photochemical loss of peripheral hydrogen atoms from the PAHs is a relatively gentle process in terms of excess energy available. As a result, the final isomerization process into carbon chains and/or rings may leave an imprinted memory of the preceding PAH skeleton. There is presently no experimental data available on the molecular structure of the final products, but we note that this may well be very relevant for studies of the DIBs (see Section 4.3.1).

Above we discuss the observed variations in the peak position of the 7.7-μm band among different objects (see Section 2.2.2). Interpreting the class A peak position as characteristic of large compact aromatic species, the shift to longer wavelengths for classes B and C may reflect the increased importance of aliphatic groups attached to the aromatic network (Sloan et al. 2007). Although this seems reasonable for class C objects with a peak position at ∼8.2 μm, this interpretation is not entirely straightforward for class B sources. Nevertheless, adopting this point of view and following the discussion above, a model emerges in which the molecular structure of the emitting species (and hence the peak positions of the bands) represents a balance between reactions with C, C^+, and H producing aliphatic groups and photodissociation of these peripheral groups (Sloan et al. 2007). The cool post-AGB objects allow the balance to shift largely to the aliphatic side. In contrast, in the ISM, the available high-energy photons rapidly strip nonaromatic groups, and the abundance of aliphatic groups is very small (see Section 3.3). As for the dehydrogenation of PAHs, this balance is sensitive to the local physical conditions (e.g., G_o/n), and for a given

PAH size, only a relatively small shift in this parameter is required. We note then that the 3.4-μm band—which traces the aliphatic component—disappears rapidly toward the surface of the Orion Bar PDR (Geballe et al. 1989, Joblin et al. 1996), supporting this active chemistry in PDRs and the sensitivity of these groups to local physical conditions.

Finally, these reactions affect only peripheral groups attached to the PAHs. No chemical route has been identified that could lead in the ISM to the incorporation of nitrogen deep into the carbon skeleton that is needed to explain the observed shift of the 6.2-μm band from class B to class A (see Section 4.2.3).

6. POLYCYCLIC AROMATIC HYDROCARBONS AND THE PHYSICS OF THE INTERSTELLAR MEDIUM

6.1. Ionization Balance

Charge has a profound effect on the IR spectral characteristics of PAHs (see Section 4.2.1). Likewise, charged PAHs have visible electronic transitions in the visible and may therefore be responsible for the DIBs. In addition, because of their large cross sections, (charged) PAH species interacting with electrons and cations can dominate the ionization balance of neutral interstellar gas (Lepp & Dalgarno 1988, Lepp et al. 1988). Specifically, the ionization balance of HI regions and PDRs is dominated by the photoionization of neutral carbon. Direct electron recombination of C^+ is radiative and hence very slow. In contrast, anions formed by electron attachment to PAHs provide an effective recombination channel for atomic cations. This influences the relative abundance of neutral and ionic species in diffuse clouds (Liszt 2003, Wolfire et al. 2008) and PDRs (Bakes & Tielens 1998), as well as the photoelectric heating rate (see Section 6.2). PAH-assisted recombination is also important in molecular clouds—now for molecular ions—and, because PAHs control the recombination rate, their presence influences the ambipolar diffusion rate and, through ion-molecule reaction schemes, the composition of molecular clouds (Lepp & Dalgarno 1988).

The ionization balance of PAHs is set by photoionization, electron attachment to neutral PAHs, electron recombination of PAH cations, mutual neutralization reactions between PAH anions and atomic or molecular cations, and (charge-exchange) reactions of neutral PAHs with cations. The past decade has seen a flurry of experiments to measure the rates of these process (see Section 5.2). A number of theoretical studies on the ionization balance involving PAHs have appeared (Bakes & Tielens 1994; Salama et al. 1996; Weingartner & Draine 2001; Le Page, Snow & Bierbaum 2003). However, such studies are only as good as the rates that go in to them, and our understanding of these processes for large PAHs is presently only rudimentary.

From an observational viewpoint, we can estimate the average recombination rate of astrophysical PAHs directly from observations (see Section 4.2.1). Assuming that the 6.2-μm and 7.7-μm bands and the 3.3-μm and 11.2-μm bands result from cations and neutrals, respectively, the intensity ratio of these bands is a direct measure of the energy absorbed by ions relative to neutrals. Assuming then also that the populations are the same, this ratio provides the ion-to-neutral fraction. For a well-studied PDR (such as the Orion Bar) in which the physical conditions are known, this can be translated into an average electron recombination rate. Assuming three ionization stages, the ionization rates appropriate for circumcoronene ($C_{54}H_{24}$), and a factor of 2 difference between the recombination rates of the ions, this analysis results in an astronomical PAH cation recombination rate of approximately 2×10^{-5} cm^3 s^{-1}. This is in line with the rate expected for a thin circular conducting disk but substantially larger than that measured for small PAHs (**Figure 18**).

The carbon ionization balance in the diffuse interstellar clouds is sensitive to the carbon charge-exchange and mutual neutralization rates. A recent analysis of available observational data suggests

rates for these processes that are approximately a factor of 2 smaller than expected based on the Langevin rate for a 50 C-atom PAH (Wolfire et al. 2008).

6.2. Photoelectric Heating

Photoelectric heating is the dominant process that couples the energy balance of the gas to the nonionizing radiation field of stars in HI regions. As such, photoelectric heating ultimately controls the physical conditions in PDRs (which include most of the HI gas mass of the ISM) and the phase structure of the ISM; therefore it controls the evolution of the ISM of galaxies (Hollenbach & Tielens 1999). It has long been recognized that photoelectric heating is dominated by the smallest grains present in the ISM and PAHs, and very small grains dominate the heating of interstellar gas. Essentially, absorption of an FUV photon creates an electron-hole pair in the material. The electron diffuses toward the surface, losing its excess kinetic energy along the way through collisions. Because the FUV absorption depth (~100 Å) can be much larger than the mean free path of low-energy electrons in solid materials, the yield is very low for large grains. Because of the Coulomb attraction, the photoelectric heating efficiency is sensitive to the grain charge (e.g., ionization potential). The charge of a species is set by the ratio of the ionization rate over the recombination rate, which is proportional to the charging parameter, $G_o T^{1/2}/n_e$ (Tielens 2005).

Bakes & Tielens (1994) and Weingartner & Draine (2001) have performed extensive theoretical calculations on the heating by an interstellar grain-size distribution of PAHs and small grains, including the effects of charge, and the resulting efficiencies (the ratio of gas heating to the FUV absorption rate of grains and PAHs) have been fitted to a simple analytical formula. **Figure 19** shows the calculated photoelectric heating rate as a function of grain size, illustrating that only species less than ~100 Å contribute effectively (Bakes & Tielens 1994). **Figure 19** also compares the calculated photoelectric efficiency as a function of the charging parameter, γ, to observations

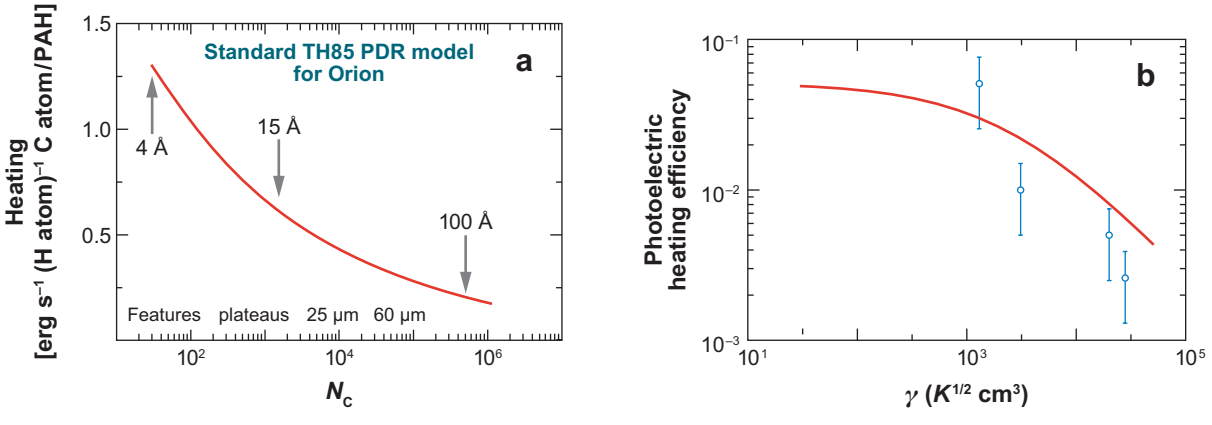

Figure 19

(*a*) The contribution to the photoelectric heating of interstellar gas by species of different sizes (Bakes & Tielens 1994). The results of these calculations are presented in such a way that equal areas under the curve correspond to equal contributions to the heating. Typically, approximately half of the heating originates from polycyclic aromatic hydrocarbons (PAHs) and PAH clusters ($<10^3$ C atoms). The other half is contributed by very small grains (15 Å $< a <$ 100 Å). Classical grains do not contribute noticeably to the heating. (*b*) The photoelectric efficiency as a function of the charging parameter, $\gamma = G_o T^{1/2}/n_e$ (proportional to the ionization rate over the recombination rate). Neutral species are located to the left, whereas to the right the charge of species increases. The data points (*blue*) indicate the measured heating efficiency for the diffuse interstellar medium sight lines ζ Oph and ξ Per and the well-studied photodissociation regions (PDRs) NGC 2023 and the Orion Bar.

of the heating in diffuse sight lines and in well-known PDRs. For the diffuse sight lines, the photoelectric heating rate is determined from the upper-level populations of the CII fine-structure transition measured through FUV absorption lines (Pottasch, Wesselius & van Duinen 1979; Gry, Lequeux & Boulanger 1992) in which the physical conditions have been taken from van Dishoeck & Black's (1986) definitive study. For PDRs, the photoelectric efficiency has been determined directly by comparing the intensity of the dominant cooling lines ([OI], [CII]) to the far-IR dust emission. Physical conditions in these regions were determined from atomic and molecular line ratios (Hollenbach & Tielens 1999). The calculated efficiency compares reasonably well to these observations. It can be expected that SOFIA and Herschel—in combination with the Atacama Large Millimeter Array—can substantially increase the sample of sources for which this comparison can be made. More importantly, because the emission spectra of PAHs are such a sensitive function of grain charge (see Section 4.2.1), combining mid-IR PAH spectra studies and far-IR gas cooling line and dust emission studies can directly test the photoelectric heating model and observationally determine its dependence on such important parameters as the local radiation field, gas temperature, electron density, and metallicity.

7. POLYCYCLIC AROMATIC HYDROCARBONS AND STAR FORMATION

7.1. Polycyclic Aromatic Hydrocarbon Characteristics in Protoplanetary Disks

The IR spectra of regions of star and planet formation are rich and diverse. With regard to isolated systems in which the emission originates from either the disk or the envelope, the spectra often show the presence of PAH emission features, as well as amorphous silicates, crystalline silicates, and, in a few cases, diamond bands (Meeus et al. 2001; Acke & van den Ancker 2004, 2006; Habart, Natta & Krügel 2004; Geers et al. 2006, 2007; Habart et al. 2006; Doucet et al. 2007). The most striking aspect of the existing samples of Herbig AeBe and T Tauri stars is that all combinations of these emission components occur: Some spectra show all emission components, others show only amorphous silicates or combinations of amorphous and crystalline silicates, and a few spectra even show only IR emission features perched on an otherwise featureless continuum. The occurrence of these different components clearly is controlled by fundamentally different processes. The presence of the IR emission features in the sample, in particular, seems to link back to the geometry of the disk-star system (Meeus et al. 2001, Acke & van den Ancker 2004), and the IR emission features are associated with systems with flaring disks likely because large portions of the disk are exposed to the UV radiation from the central star. The silicate feature, conversely, does not show such a pronounced correlation with geometry.

Recent ground-based studies—in particular using adaptive optics techniques with resolutions of ∼0.1″—have revealed that the IR emission features originate from regions with radii of 10 to 60 AU (Habart et al. 2006, Doucet et al. 2007, Geers et al. 2007). Typically, the IR emission features are more extended than the underlying continuum, but there are known exceptions. The prototypical isolated Herbig star HD 100546 shows evidence of a 5–10 AU gap, and the 3.3-μm emission feature may be associated with the outer rim of this gap (Geers et al. 2007).

The strength of the IR emission features is generally much weaker relative to the total IR emission in Herbig star spectra than in the diffuse ISM. Moreover, the strength decreases with stellar effective temperature, and no T Tauri stars of spectral type later than G8 show the IR emission features in their spectra (**Figure 20**). A simple model shows that the observations are consistent with a 50/50 mixture of neutral and ionized 100 C-atom PAHs—approximately twice the average size in the diffuse ISM—with an abundance reduced by a factor of 10 to 100 (see **Figure 20**). Both trends (increased size/decreased abundance) have been attributed to the photodissociation

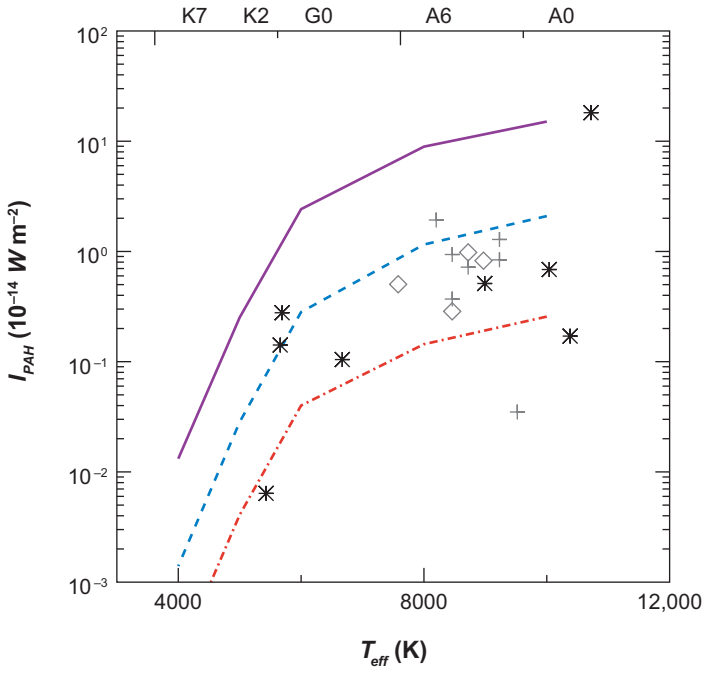

Figure 20

The strength of the 11.2-μm feature scaled to a source distance of 150 pc as a function of the effective temperature of the star. Gray points are Herbig stars observed by the Infrared Space Observatory, and asterisks denote T Tauri stars observed by Spitzer. Curves present model results for disks with interstellar medium (*purple*) abundances and 10 times (*blue dashed*) and 100 times (*red dot-dashed*) lower polycyclic aromatic hydrocarbon (PAH) abundance. Figure taken from Geers et al. 2006.

of PAHs in the intense radiation field due to the central star (Visser et al. 2007), possibly because of multiphoton effects in the intense stellar radiation field. Alternatively, the decreased strength of the IR emission features in these objects and, particularly, the disappearance in stars with spectral types later than G8 may reflect the low efficiency of visible photons in exciting PAHs (Visser et al. 2007). Indeed, post-AGB stars show much weaker IR emission features in their spectra if the exciting star is as cool as G (Buss et al. 1990, 1993). Likewise, reflection nebulae cooler than 7000 K show weak if any IR emission features in their spectra (Sellgren, Luan & Werner 1990; Uchida et al. 2000; Li & Draine 2002).

Finally, above we discussed the peak position of the 7.7-μm band in regions of star formation (see Section 2.2.2). The observed rapid transition of the peak position of the 7.7-μm band in the spectra of Herbig stars and T Tauri stars implies an active chemistry controlled by the local physical conditions in these sources, for example, owing to a shift in the balance between hydrogen photodissociation and hydrogen-addition reactions (see Section 5.4.3).

7.2. Polycyclic Aromatic Hydrocarbons as Tracers of Star Formation

The ubiquity of the PAH emission features and their predominance in the mid-IR spectra of massive star-forming regions (see **Figure 2**) make them potentially powerful tools for the study of star formation throughout the universe. Essentially, the PAHs act as a dye for the presence of pumping FUV photons and hence trace the presence of massive stars. Genzel et al. (1998)

have already employed this aspect of IR emission features to conclude that ULIRGs are largely powered by star formation rather than active galactic nucleus activity. Whereas ISO was able to probe these emission features in the local universe (out to red shifts of ∼0.1), with Spitzer, the use of the IR emission features as probes of star formation has been extended to $z \sim 3$ for lensed galaxies and luminous submillimeter galaxies (Lutz et al. 2007, Pope et al. 2007, Rigby et al. 2007). Ultimately, the James Webb Space Telescope is expected to open up the whole universe to studies of the IR emission features as tracers of star formation. Of course, this all rests on the validation and quantification of the relationship between the IR emission features and the star-formation rate.

Calzetti et al. (2007) have addressed this relationship based on the Spitzer infrared array camera 8-μm (PAH) and HST-NICMOS (Pα) images of (part of) the SINGS sample of galaxies, as well as low-metallicity starburst galaxies and luminous infrared galaxies. They find an almost linear correlation between the PAH emission and the ionizing photon rate for galaxies with metallicities close to the solar value. However, in the wider sample, this relationship shows a strong dependence on metallicity and size, as well as possibly star-formation history (see Section 3.9). A combination of 24-μm Spitzer MIPS and Hα data provides a good handle on the star-formation rate in these types of galaxies: Extinction in the inner galaxy hampers the use of Hα, whereas the outer galaxy is optically thin in the dust, and the IR underestimates the star-formation rate.

From a different perspective, the ISO-SWS sample of HII regions is well suited to calibrate the relationship between the IR emission features and massive star formation (**Figure 21**). The good relationship of the 6.2-μm PAH/far-IR and the 6.2-μm continuum/far-IR ratios ranges from deeply embedded compact HII regions (such as W3) to exposed PDRs (such as the Orion Bar and the reflection nebula NGC 2023), and the diffuse ISM (such the IR cirrus and the surfaces of dark clouds). Obviously, there is a correlation between the strength of the 6.2-μm IR emission feature and the 6.2-μm continuum, ignoring the obvious outliers, typically to a factor of 4 (which is actually about the range of the 6.2-μm-continuum variations in the sample of ULIRGs and starburst nuclei). In addition, both the 6.2-μm feature and the local continuum vary relative to the far-IR continuum by orders of magnitude (**Figure 21**).

In this sample of HII regions, the strength of the 6.2-μm feature clearly does not provide a good measure of the total IR luminosity produced by star formation. The variation in the PAH/far-IR ratio is correlated with the characteristics of the source. Exposed PDRs—such as the Orion Bar, NGC 2023, and the diffuse ISM—all have relatively high ratios, whereas deeply embedded HII regions have low ratios. **Figure 22** presents this effect in a slightly different way. The increased FUV field incident on PDRs associated with more compact HII regions possibly destroys small PAHs (see Section 5.1). Alternatively, more of the FUV is absorbed by dust inside the HII region and never reaches the PAHs in the PDRs (see Section 3.4). Therefore, if the characteristics of the regions of massive star formation do not change within an extragalactic sample, the PAH emission scales with the IR luminosity and provides a tracer of star formation (Pope et al. 2007). However, quantifying a PAH flux—e.g., measured for local ULIRGs or with the James Webb Space Telescope in the far universe—into a star-formation rate requires knowledge of the star-formation characteristics and/or identification of appropriate local templates (Peeters, Spoon & Tielens 2004). Besides the Genzel diagram, other diagnostic diagrams have been employed using color temperatures, for example, and their interpretation is generally based on the use of relevant templates (see Laurent et al. 2000). The templates used of course steer the result. In that respect, ultracompact HII regions, such as NGC 7538-IRS 1 and K3-50A, are always problematic (**Figure 21**). Additionally, none of these attempts captures the phase of deeply embedded star formation—characterized by molecular absorption lines rather than PAH emission features—yet this phase may last much longer in the high-pressure environment of starburst galactic nuclei (Lahuis et al. 2007).

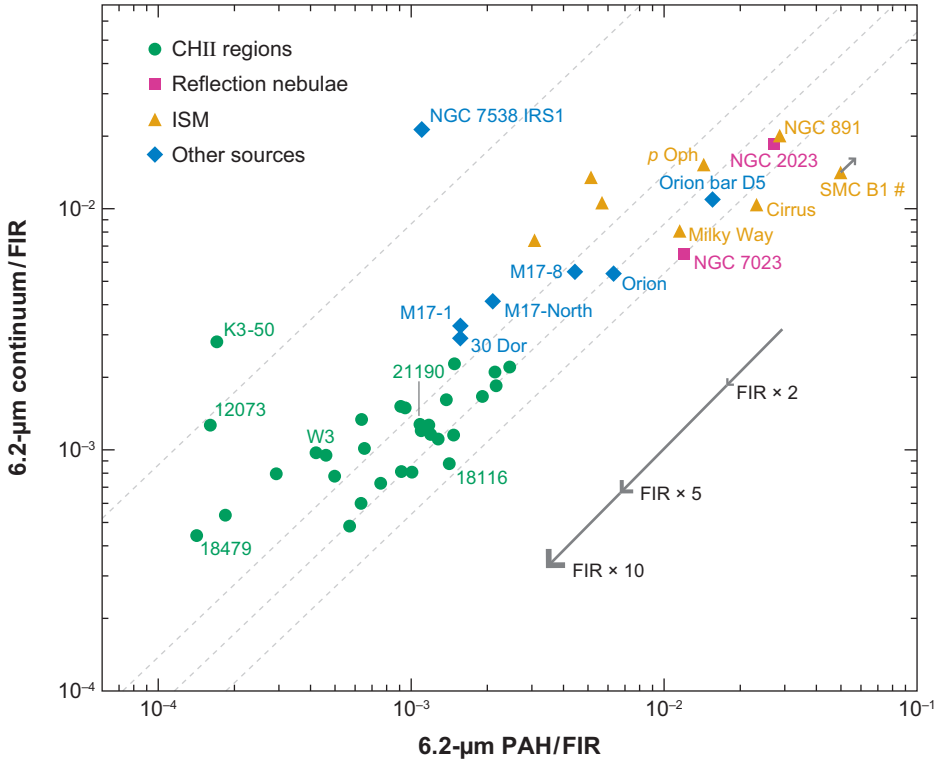

Figure 21

The ratio of the 6.2-μm infrared emission feature to the far-infrared (FIR) continuum emission compared with the ratio of the 6.2-μm continuum to the FIR continuum for a sample of galactic HII regions, reflection nebulae, and diffuse interstellar medium (ISM) sources (Peeters, Spoon & Tielens 2004). The dotted lines correspond to 6.2-μm polycyclic aromatic hydrocarbon (PAH) continuum ratios of (*from left to right*) 0.116, 0.72, 1.16, and 1.85.

8. EPILOGUE

Over the past 20 years it has become increasingly clear that we live in a molecular universe: Molecules are directly interwoven into the fabric of the universe. They are an important component of the universe and play a central role in many key processes that dominate the structure and evolution of the ISM of galaxies, not only in the here and now but all the way back to first starlight in the universe. Understanding the origin and evolution of interstellar molecules and their role in the universe is therefore a fundamental goal of modern astrophysics.

This review highlights the progress made, observationally and theoretically, in understanding the role of PAHs in the ISM of galaxies over the past 20 years. Large PAH molecules are abundant and ubiquitous in the ISM of galaxies. They control the heating of the gas and the degree of ionization in the ISM. Observationally, PAHs are the extension of the interstellar grain-size distribution into the molecular domain. They either may be the leftover dust condensation nuclei that escaped the grain growth process in AGB ejecta or they could be formed through shattering collisions in fast interstellar shocks; likely, both premises are correct. Large molecules may well be an important catalytic source of small carbon radicals in interstellar clouds, reflecting a

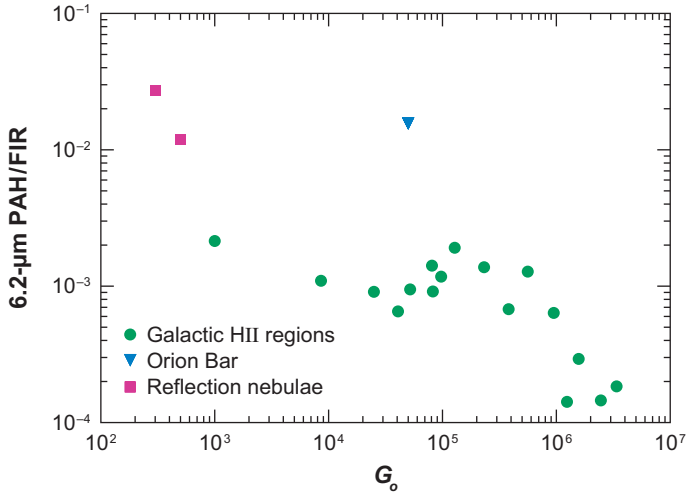

Figure 22

The observed strength of the 6.2-μm band relative to the far-infrared (FIR) dust-continuum emission plotted as a function of the intensity of the incident far-ultraviolet field, G_o, in Habing units. The squares and triangle correspond to the bright photodissociation regions (PDRs) associated with the Orion Bar, NGC 2023, and NGC 7023. G_o has been estimated from the observed FIR flux assuming that the IR emission features originate in the PDR, whose distance from the illuminating star is given by the radio-continuum size. Figure taken from Peeters, Spoon & Tielens 2004.

balance of carbon-addition reactions and UV photolysis. Many ideas glimpsed from the literature and sprinkled through this review require further observational, experimental, and theoretical validation. Among the questions that the field should focus on in the coming decade are, what are the spectroscopic signatures of large PAH molecules, and how do they depend on the molecular structure? What is the relationship between the chemical and physical characteristics of large molecules (e.g., size, charge state, excitation) and the physical conditions of a region (e.g., density, temperature, radiation field, metallicity)? How can we translate these observational characteristics into astronomers' tools to reveal the physical conditions in regions near and far? What is the role of PAHs in creating the molecular diversity of the ISM, and what are the key (photo)chemical reactions that link large PAHs to carbon chains in the ISM?

Eddington, after the discovery of the first diatomic molecules, exclaimed that "atoms are physics but molecules are chemistry." He meant of course that whereas one might hope to capture the universe in simple laws as long as atoms rule, with molecules, the impure solutions of chemistry take control. I do not share this concern. Molecules provide unique and novel ways to probe the universe and its inner workings. With SOFIA, Herschel, and the James Webb Space Telescope missions around the corner, we can expect that these opportunities will be utilized in the near future to the fullest. With the dedicated efforts of some of the world's leading physics and chemistry laboratories, I can say that the universe is only now truly wide open.

DISCLOSURE STATEMENT

The author is not aware of any biases that might be perceived as affecting the objectivity of this review.

ACKNOWLEDGEMENTS

I would like to thank Els Peeters, Sacha Hony, Caroline van Kerckhoven, Henrik Spoon, and Christiaan Boersma for their dedicated efforts in analyzing and interpreting the ISO SWS and Spitzer IRS data on interstellar PAHs and their willingness to share these exciting times with me. Special thanks to Els and Sacha, as well as to Jan Cami and Olivier Berne, for providing some of the figures in this review. I am deeply indebted to Ewine van Dishoeck and Christine Joblin for their careful reading of an earlier version of this manuscript. I also thank Lou Allamandola for sharing his insights on PAHs over these past 20 years.

LITERATURE CITED

Abergel A, Bernard JP, Boulanger F, Cesarsky D, Falgarone E, et al. 2002. *Astron. Astrophys.* 389:239
Abouelaziz JC, Gomet JC, Pasquerault D, Rowe BR, Mitchell JBA. 1993. *Chem. Phys.* 99:237
Acke B, van den Ancker ME. 2004. *Astron. Astrophys.* 426:151
Acke B, van den Ancker ME. 2006. *Astron. Astrophys.* 457:171
Allain T, Leach S, Sedlmayr E. 1996. *Astron. Astrophys.* 305:602
Allamandola LJ, Hudgins DM, Bauschlicher CW Jr, Langhoff SR. 1999. *Astron. Astrophys.* 352:659
Allamandola LJ, Hudgins DM, Sandford SA. 1999. *Ap. J.* 511:L115
Allamandola LJ, Tielens AGGM, Barker JR. 1985. *Ap. J.* 290:L25
Allamandola LJ, Tielens AGGM, Barker JR. 1989. *Ap. J. Suppl.* 71:733
Armus L, Charmandaris V, Bernard-Salas J, Spoon HWW, Marshall JA, et al. 2007. *Ap. J.* 656:148
Bakes ELO, Tielens AGGM. 1994. *Ap. J.* 427:822
Bakes ELO, Tielens AGGM. 1998. *Ap. J.* 499:258
Bakes ELO, Tielens AGGM, Bauschlicher CW Jr. 2001. *Ap. J.* 556:501
Bakes ELO, Tielens AGGM, Bauschlicher CW Jr, Hudgins DM, Allamandola LJ. 2001. *Ap. J.* 560:261
Barker JR, Allamandola LJ, Tielens AGGM. 1987. *Ap. J.* 315:L61
Bauschlicher C, Bakes ELO. 2000. *Chem. Phys.* 4:24
Bauschlicher CW Jr. 2002. *Ap. J.* 564:782
Bauschlicher CW Jr, Peeters E, Allamandola LJ. 2008. *Ap. J.* 678:316
Berné O, Joblin C, Deville Y, Smith JD, Rapacioli M, et al. 2007. *Astron. Astrophys.* 469:575
Berné O, Joblin C, Rapacioli M, Thomas J, Cuillandre J-C, Deville Y. 2008. *Astron. Astrophys.* 479:L41
Bernstein MP, Elsila JE, Dworkin JP, Sandford SA, Allamandola LJ, Zare RN. 2002. *Ap. J.* 576:1115
Bernstein MP, Sandford SA, Allamandola LJ. 1996. *Ap. J.* 472:L127
Bettens RPA, Herbst E. 1997. *Ap. J.* 478:585
Betts NB, Stepanovic M, Snow TP, Bierbaum VM. 2006. *Ap. J.* 651:L129
Biennier L, Alsayed-Ali M, Foutel-Richard A, Novotny O, Carles S, et al. 2006. *Discuss. Faraday Soc.* 133:289
Boersma C, Hony S, Tielens AGGM. 2006. *Astron. Astrophys.* 447:213
Bohme DK. 1992. *Chem. Rev.* 92:1487
Brandl BR, Bernard-Salas J, Spoon HWW, Devost D, Sloan GC, et al. 2006. *Ap. J.* 653:1129
Bréchignac P, Pino T. 1999. *Astron. Astrophys.* 343:L49
Bréchignac P, Schmidt M, Masson A, Pino T, Parneix P, Brechignac C. 2005. *Astron. Astrophys.* 442:239
Bregman JD, Allamandola LJ, Witteborn FC, Tielens AGGM, Geballe TR. 1989. *Ap. J.* 344:791
Bregman J, Temi P. 2005. *Ap. J.* 621:831
Burton MG, Ashley MCB, Marks RD, Schinckel AE, Storey JWV, et al. 2000. *Ap. J.* 542:359
Buss RH Jr, Cohen M, Tielens AGGM, Werner MW, Bregman JD, et al. 1990. *Ap. J.* 365:L23
Buss RH Jr, Tielens AGGM, Cohen M, Werner MW, Bregman JD, Witteborn FC. 1993. *Ap. J.* 415:250
Buss RH Jr, Tielens AGGM, Snow TP. 1991. *Ap. J.* 372:281
Calzetti D, Kennicutt RC, Engelbracht CW, Leitherer C, Draine BT, et al. 2007. *Ap. J.* 666:870
Canosa A, Laubé S, Rebrion C, Pasquerault D, Gomet JC, Rowe BR. 1995. *Chem. Phys. Lett.* 245:407
Canosa A, Parent DC, Pasquerault D, Gomet JC, Laubé S, Rowe BR. 1994. *Chem. Phys. Lett.* 228:26
Cau P. 2002. *Astron. Astrophys.* 392:203

Cernicharo J. 2004. *Ap. J.* 608:L41
Cernicharo J, Heras AM, Tielens AGGM, Pardo JR, Herpin F, et al. 2001. *Ap. J.* 546:L123
Cherchneff I, Barker JR, Tielens AGGM. 1992. *Ap. J.* 401:269
Cesarsky D, Lequeux J, Ryter C, Gérin M. 2000. *Astron. Astrophys.* 354:L87
Cook DJ, Saykally RJ. 1998. *Ap. J.* 493:793
Cook DJ, Schlemmer S, Balucani N, Wagner DR, Harrison JA, et al. 1998. *J. Phys. Chem. A* 102:1465
de Frees DJ, Miller MD, Talbi D, Pauzat F, Ellinger Y. 1993. *Ap. J.* 408:530
Desert F-X, Boulanger F, Puget JL. 1990. *Astron. Astrophys.* 237:215
Doucet C, Habart E, Pantin E, Dullemond C, Lagage PO, et al. 2007. *Astron. Astrophys.* 470:625
Douglas AE. 1977. *Nature* 269:130
Draine BT, Dale DA, Bendo G, Gordon KD, Smith JDT, et al. 2007. *Ap. J.* 663:866
Draine BT, Lazarian A. 1998. *Ap. J.* 508:157
Draine BT, Li A. 2001. *Ap. J.* 551:807
Draine BT, Li A. 2007. *Ap. J.* 657:810
Engelbracht CW, Gordon KD, Rieke GH, Werner MW, Dale DA, Latter WB. 2005. *Ap. J.* 628:L29
Engelbracht CW, Kundurthy P, Gordon KD, Rieke GH, Kennicutt RC, et al. 2006. *Ap. J.* 642:L127
Flagey N, Boulanger F, Verstraete L, Miville Deschênes MA, Noriego Crespo A, et al. 2006. *Astron. Astrophys.* 453:969
Frenklach M, Feigelson ED. 1989. *Ap. J.* 341:372
Galliano F, Dwek E, Chanial P. 2008. *Ap. J.* 672:214
Galliano F, Madden SC, Tielens AGGM, Peeters E, Jones AP. 2008. *Ap. J.* 679:310
Geballe TR, Tielens AGGM, Allamandola LJ, Moorhouse A, Brand PWJL. 1989. *Ap. J.* 341:278
Geers VC, Augereau J-C, Pontoppidan KM, Dullemond CP, Visser R, et al. 2006. *Astron. Astrophys.* 459:545
Geers VC, van Dishoeck EF, Visser R, Pontoppidan KM, Augereau J-C, et al. 2007. *Astron. Astrophys.* 476:279
Geers VC. 2007. PhD thesis. Univ. of Leiden
Genzel R, Lutz D, Sturm E, Egami E, Kunze D, et al. 1998. *Ap. J.* 498:579
Gotkis Y, Oleinikova M, Naor M, Lifshitz C. 1993. *J. Phys. Chem.* 97:12282
Goulay F, Rebrion-Rowe C, Biennier L, Le Picard SD, Canosa A, Rowe BR. 2006. *J. Phys. Chem. A* 110:3132
Goulay F, Rebrion-Rowe C, Le Garrec JL, Le Picard SD, Canosa A, Rowe BR. 2005. *J. Chem. Phys.* 122:104308
Gry C, Lequeux J, Boulanger F. 1992. *Astron. Astrophys.* 266:457
Habart E, Natta A, Krügel E. 2004. *Astron. Astrophys.* 427:179
Habart E, Natta A, Testi L, Carbillet M. 2006. *Astron. Astrophys.* 449:1067
Herbig GH. 1975. *Ap. J.* 196:129
Herbig GH. 1995. *Annu. Rev. Astron. Astrophys.* 33:19
Hollenbach DJ, Tielens AGGM. 1999. *Rev. Mod. Phys.* 71:173
Hony S, Van Kerckhoven C, Peeters E, Tielens AGGM, Hudgins DM, Allamandola LJ. 2001. *Astron. Astrophys.* 370:1030
Hudgins DM, Allamandola LJ. 1999a. *Ap. J.* 513:L69
Hudgins DM, Allamandola LJ. 1999b. *Ap. J.* 516:L41
Hudgins DM, Bauschlicher CW Jr, Allamandola LJ. 2005. *Ap. J.* 632:316
Huneycutt AJ, Casaes RN, McCall BJ, Chung C-Y, Lee Y-P, Saykally RJ. 2004. *Chem. Phys. Chem.* 5:321
Joblin C. 2003. In *SF2A-2003: Semaine de l'Astrophysique Francaise*, ed. F Combes, D Barret, T Contini, L Pagani. p. 175. Les Ulis, France: EdP Sci., Conf. Ser.
Joblin C, Abergel A, Bregman J, D'Hendecourt L, Heras AM, et al. 2000. In *ISO Beyond the Peaks: The 2nd ISO Workshop on Analytical Spectroscopy*, ed. A Salama, MF Kessler, K Leech, B Schulz. 456:49
Joblin C, Tielens AGGM, Allamandola LJ, Geballe TR. 1996. *Ap. J.* 458:610
Jochims HW, Baumgärtel H, Leach S. 1996. *Astron. Astrophys.* 314:1003
Jochims HW, Baumgärtel H, Leach S. 1999. *Ap. J.* 512:500
Jochims HW, Ruhl E, Baumgärtel H, Tobita S, Leach S. 1994. *Ap. J.* 420:307
Jolibois F, Klotz A, Gadéa FX, Joblin C. 2005. *Astron. Astrophys.* 444:629
Jones AP, Tielens AGGM, Hollenbach DJ. 1996. *Ap. J.* 469:740
Kim H-S, Saykally RJ. 2002. *Ap. J. Suppl.* 143:455
Kim H-S, Wagner DR, Saykally RJ. 2001. *Phys. Rev. Lett.* 86:5691

Klotz A, Marty P, Boissel P, Serra G, Chaudret B, Daudey JP. 1995. *Astron. Astrophys.* 304:520
Kogut A, Banday AJ, Bennett CL, Gorski KM, Hinshaw G, Reach WT. 1996. *Ap. J.* 460:1
Lahuis F, Spoon HWW, Tielens AGGM, Doty SD, Armus L, et al. 2007. *Ap. J.* 659:296
Langhoff S. 1996. *J. Phys. Chem.* 100:2819
Latter WB. 1991. *Ap. J.* 377:187
Laurent O, Mirabel IF, Charmandaris V, Gallais P, Madden SC, et al. 2000. *Astron. Astrophys.* 359:887
Leach S. 1987. In *NATO ASIC Proc. 191: Polycyclic Aromatic Hydrocarbons and Astrophysics*, ed. A Leger, p. 99. Dordrecht: Reidel
Le Page V, Keheyan Y, Snow TP, Bierbaum VM. 1999a. *Int. J. Mass Spectrom.* 185:949
Le Page V, Keheyan Y, Snow TP, Bierbaum VMl. 1999b. *J. Am. Chem. Soc.* 121:9435
Le Page V, Snow TP, Bierbaum VM. 2001. *Ap. J. Suppl.* 132:233
Le Page V, Snow TP, Bierbaum VM. 2003. *Ap. J.* 584:316
Lepp S, Dalgarno A. 1988. *Ap. J.* 324:553
Lepp S, Dalgarno A, van Dishoeck EF, Black JH. 1988. *Ap. J.* 329:418
Li A, Draine BT. 2002. *Ap. J.* 572:232
Linsky JL, Draine BT, Moos HW, Jenkins EB, Wood BE, et al. 2006. *Ap. J.* 647:1106
Liszt H. 2003. *Astron. Astrophys.* 398:621
Lorenz U, Solca N, Lemaire J, Maitre P, Dopfer O. 2007. *Angew. Chem. Int. Ed. Engl.* 46:6714
Low FJ, Young E, Beintema DA, Gautier TN, Beichman CA, et al. 1984. *Ap. J.* 278:L19
Lutz D, Sturm E, Tacconi LJ, Valiante E, Schweitzer M, et al. 2007. *Ap. J.* 661:L25
Madden SC, Galliano F, Jones AP, Sauvage M. 2006. *Astron. Astrophys.* 446:877
Maier JP, Boguslavskiy AE, Ding H, Walker GAH, Bohlender DA. 2006. *Ap. J.* 640:369
Maier JP, Walker GAH, Bohlender DA. 2004. *Ap. J.* 602:286
Malloci G, Joblin C, Mulas G. 2007a. *Astron. Astrophys.* 462:627
Malloci G, Joblin C, Mulas G. 2007b. *Chem. Phys.* 332:353
Manske V, Henning T. 1999. *Astron. Astrophys.* 349:907
Mattila K, Lemke D, Haikala LK, Laureijs RJ, Leger A, et al. 1996. *Astron. Astrophys.* 315:L353
Meeus G, Waters LBFM, Bouwman J, van den Ancker ME, Waelkens C, Malfait K. 2001. *Astron. Astrophys.* 365:476
Moutou C, Leger A, D'Hendecourt L. 1996. *Astron. Astrophys.* 310:297
Moutou C, Sellgren K, Verstraete L, Leger A. 1999. *Astron. Astrophys.* 347:949
Moutou C, Verstraete L, Leger A, Sellgren K, Schmidt W. 2000. *Astron. Astrophys.* 354:L17
Mulas G, Malloci G, Joblin C, Toublanc D. 2006a. *Astron. Astrophys.* 456:161
Mulas G, Malloci G, Joblin C, Toublanc D. 2006b. *Astron. Astrophys.* 460:93
Oomens J, Sartakov BG, Tielens AGGM, Meijer G, von Helden G. 2001. *Ap. J.* 560:L99
Oomens J, Tielens AGGM, Sartakov BG, von Helden G, Meijer G. 2003. *Ap. J.* 591:968
Oomens J, van Roij AJA, Meijer G, von Helden G. 2000. *Ap. J.* 542:404
Pauzat F, Talbi D, Ellinger Y. 1997. *Astron. Astrophys.* 319:318
Pech C, Joblin C, Boissel P. 2002. *Astron. Astrophys.* 388:639
Peeters E, Allamandola LJ, Bauschlicher CW Jr, Hudgins DM, Sandford SA, Tielens AGGM. 2004a. *Ap. J.* 604:252
Peeters E, Hony S, Van Kerckhoven C, Tielens AGGM, Allamandola LJ, et al. 2002. *Astron. Astrophys.* 390:1089
Peeters E, Mattioda AL, Hudgins DM, Allamandola LJ. 2004b. *Ap. J.* 617:L65
Peeters E, Spoon HWW, Tielens AGGM. 2004. *Ap. J.* 613:986
Peeters Z, Botta O, Charnley SB, Kisiel Z, Kuan Y-J, Ehrenfreund P. 2005. *Astron. Astrophys.* 433:583
Pety J, Teyssier D, Fossé D, Gerin M, Roueff E, et al. 2005. *Astron. Astrophys.* 435:885
Piest H, von Helden G, Meijer G. 1999. *Ap. J.* 520:L75
Pirali O, Van-Oanh N-T, Parneix P, Vervloet M, Bréchignac P. 2006. *Phys. Chem. Chem. Phys.* 8:3707
Pope A, Chary R-R, Alexander DM, Armus L, Dickinson M, et al. 2007. Preprint (arXiv:0711.1553)
Pottasch SR, Wesselius PR, van Duinen RJ. 1979. *Astron. Astrophys.* 74:L15
Puget JL, Leger A. 1989. *Annu. Rev. Astron. Astrophys.* 27:161
Rapacioli M, Calvo F, Joblin C, Parneix P, Toublanc D, Spiegelman F. 2006. *Astron. Astrophys.* 460:519
Rapacioli M, Calvo F, Spiegelman F, Joblin C, Wales DJ. 2005. *J. Phys. Chem. A* 109:2487

Rapacioli M, Joblin C, Boissel P. 2005. *Astron. Astrophys.* 429:193
Reach WT, Rho J, Tappe A, Pannuti TG, Brogan CL, et al. 2006. *Astron. J.* 131:1479
Regan MW, Thornley MD, Bendo GJ, Draine BT, Li A, et al. 2004. *Ap. J. Suppl.* 154:204
Rigby JR, Marcillac D, Egami E, Rieke GH, Richard J, et al. 2007. Preprint (arXiv:0711.1902)
Rouan D, Leger A, Omont A, Giard M. 1992. *Astron. Astrophys.* 253:498
Ruiterkamp R, Halasinski T, Salama F, Foing BH, Allamandola LJ, et al. 2002. *Astron. Astrophys.* 390:1153
Ruiterkamp R, Peeters Z, Moore MH, Hudson RL, Ehrenfreund P. 2005. *Astron. Astrophys.* 440:391
Salama F, Bakes ELO, Allamandola LJ, Tielens AGGM. 1996. *Ap. J.* 458:621
Salama F, Galazutdinov GA, Krełowski J, Allamandola LJ, Musaev FA. 1999. *Ap. J.* 526:265
Schlemmer S, Cook DJ, Harrison JA, Wurfel B, Chapman W, Saykally RJ. 1994. *Science* 265:1686
Schutte WA, Tielens AGGM, Allamandola LJ. 1993. *Ap. J.* 415:397
Sellgren K. 1984. *Ap. J.* 277:623
Sellgren K, Luan L, Werner MW. 1990. *Ap. J.* 359:384
Sellgren K, Uchida KI, Werner MW. 2007. *Ap. J.* 659:1338
Simon A, Joblin C. 2007. *J. Phys. Chem. A* 111:9745
Sloan GC, Bregman JD, Geballe TR, Allamandola LJ, Woodward CE. 1997. *Ap. J.* 474:735
Sloan GC, Jura M, Duley WW, Kraemer KE, Bernard-Salas J, et al. 2007. *Ap. J.* 664:1144
Smith D, Spanel P, Mark TD. 1993. *Chem. Phys. Lett.* 213:202
Smith JDT, Draine BT, Dale DA, Moustakas J, Kennicutt RC Jr, et al. 2007. *Ap. J.* 656:770
Snow TP, Le Page V, Keheyan Y, Bierbaum VM. 1998. *Nature* 391:259
Soifer BT, Helou G, Werner M. 2008. *Annu. Rev. Astron. Astrophys.* 46:201–40
Speck AK, Barlow MJ. 1997. *Astrophys. Space Sci.* 251:115
Szczepanski J, Vala M. 1993. *Ap. J.* 414:646
Szczepanski J, Wang H, Vala M, Tielens AGGM, Eyler JR, Oomens J. 2006. *Ap. J.* 646:666
Tappe A, Rho J, Reach WT. 2006. *Ap. J.* 653:267
Teyssier D, Fossé D, Gerin M, Pety J, Abergel A, Roueff E. 2004. *Astron. Astrophys.* 417:135
Thaddeus P. 1995. See Tielens & Snow 1995, p. 369
Thorwirth S, Theulé P, Gottlieb CA, McCarthy MC, Thaddeus P. 2007. *Ap. J.* 662:1309
Tielens AGGM, ed. 2005. *The Physics and Chemistry of the Interstellar Medium*. Cambridge, UK: Cambridge Univ. Press
Tielens AGGM, Meixner MM, van der Werf PP, Bregman J, Tauber JA, et al. 1993. *Science* 262:86
Tielens AGGM, Snow TP, eds. 1995. *The Diffuse Interstellar Bands*. Dordrecht: Kluwer Acad.
Tobita S, Meinke M, Illenberger E, Christophorous LG, Baumgärtel H, Leach S. 1992. *Chem. Phys.* 161:501
Uchida KI, Sellgren K, Werner MW, Houdashelt ML. 2000. *Ap. J.* 530:817
van Diedenhoven B, Peeters E, Van Kerckhoven C, Hony S, Hudgins DM, et al. 2004. *Ap. J.* 611:928
van Dishoeck EF, Black JH. 1986. *Ap. J. Suppl.* 62:109
Van Kerckhoven C. 2002. PhD thesis. Catholic Univ. Leuven, Belgium
Van Kerckhoven C, Hony S, Peeters E, Tielens AGGM, Allamandola LJ, et al. 2000. *Astron. Astrophys.* 357:1013
Verstraete L, Leger A, D'Hendecourt L, Defourneau D, Dutuit O. 1990. *Astron. Astrophys.* 237:436
Verstraete L, Pech C, Moutou C, Sellgren K, Wright CM, et al. 2001. *Astron. Astrophys.* 372:981
Verstraete L, Puget JL, Falgarone E, Drapatz S, Wright CM, Timmermann R. 1996. *Astron. Astrophys.* 315:L337
Visser R, Geers VC, Dullemond CP, Augereau J-C, Pontoppidan KM, van Dishoeck EF. 2007. *Astron. Astrophys.* 466:229
Wagner DR, Kim H, Saykally RJ. 2000. *Ap. J.* 545:854
Weingartner JC, Draine BT. 2001. *Ap. J. Suppl.* 134:263
Werner MW, Uchida KI, Sellgren K, Marengo M, Gordon KD, et al. 2004. *Ap. J. Suppl.* 154:309
Whittet DCB, Boogert ACA, Gerakines PA, Schutte W, Tielens AGGM, et al., 1997. *Ap. J.* 490:729
Wolfire MG, Tielens AGGM, Hollenbach D, Kaufman MJ. 2008. *Ap. J.* 680:384
Woods PM, Millar TJ, Zijlstra AA, Herbst E. 2002. *Ap. J.* 574:L167
Wu Y, Charmandaris V, Hao L, Brandl BR, Bernard-Salas J, et al. 2006. *Ap. J.* 639:157
Zacharia R. 2004. PhD thesis. Freien Universität Berlin

Annual Review of Astronomy and Astrophysics

Volume 46, 2008

Contents

Indexes

Errata

An online log of corrections to *Annual Review of Astronomy and Astrophysics* articles may be found at http://astro.annualreviews.org/errata.shtml